Experimental investigation on the use of multiple very low-cost inertial-based devices for comfort assessment and rail track monitoring

Rafael Henrique de Oliveira, Giuseppe Loprencipe, Flavio Guilherme Vaz de Almeida Filho, Rodrigo de Sousa Pissardini

ABSTRACT

The periodic rail track inspection is mandatory to ensure ride comfort and operational safety. However, conventional monitoring technologies have high costs, stimulating research on low-cost alternatives. In this regard, this paper presents the first experimental results on the use of multiple very low-cost sensors aboard trains for vibration monitoring, proposing a collective approach to provide more accurate and robust results. Nine devices comprising commercial-grade inertial sensors were tested in different distributions aboard a track recording train. Frequency weighted accelerations were calculated in accordance with ISO 2631 standard as comfort and indirect track quality index. As expected, vertical and lateral results were correlated with, respectively, track longitudinal level (range D1, maximum correlation coefficient of 0.86) and alignment (range D2, maximum correlation coefficient of 0.60), with numerically similar results when considered the fused signal. The potentiality of the collective approach was proven as result of noise reduction and identification of discrepant sensors.

Keywords

Collective monitoring; ride comfort analysis; rail track monitoring; Inertial Measurement Unit; multi-sensor data fusion

1 Introduction

For railway infrastructure management, the periodic inspection of track quality is fundamental to ensure proper dynamic behaviour of the train-track system and, thus, a safe operation and a comfortable ride. For this inspection activity, the use of dedicated self-propelled or hauled vehicles, such as track recording (or track geometry) cars and trains, is a well-established technique [1–4] and a more productive alternative to the traditional survey with topographic instruments, the visual inspection, and the manual track geometry trolleys.

In order to fit the inspection activity to average running speeds even in high-speed lines, the most modern track recording vehicles technologies mainly employ optical system (noncontact) and inertial sensors (response-based) to gather geometry data [4,5], i.e., the surveying of designed geometry and its defects/irregularities. Examples of these concepts are the modern track recording trains that are similarly designed or converted from commercial passenger trains or coaches [3,6,7]. These dedicated vehicles may carry dozens of sensors comprising optical lasers and inertial platforms for track inspections, strap-down inertial sensors to perform running behaviour and ride comfort, and complementary sensors to perform signalling, catenary, and telecommunication inspection. More affordable alternatives are the Unattended Geometry Measuring Systems (UGMS), compact modules that combine inertial sensors and laser triangulation surveying and are able to be installed underneath commercial trains [8].

The main drawbacks of dedicated track inspection vehicles and systems are their high acquisition and maintenance costs, and the significant traffic impact. These factors hinder a regular, frequent cycle of inspections and curbs continuous or quasi-continuous monitoring, stimulating the search for alternative methods with lower costs. Alternatives such as the UGMS modules do not impact traffic but still demands a considerable investment of resources. Pursuing even lower costs and quasi-continuous monitoring, alternatives have arisen based on low-cost, small-size inertial sensors attached in the axle box [9–14], the bogie [15–18], or the car body [19–22] of in-service vehicles to measure vibration response to track irregularities. As an example of commercial application of this concept, Deutsche Bahn employs inertial sensors installed in the restaurant car

of high-speed trains to perform track geometry, running behaviour and ride comfort assessment in complement to the inspection already performed by the standard track recording cars [3].

Although these proposed inertial-based systems mainly employ industrial or navigation-grade strap-down inertial sensors due to minimum performance requirements, the use of very-low-cost sensors (consumer-grade) such as those embedded in smartphones in rail track monitoring has becoming considered [20,21,23,24], laying the groundwork for collective sensing activities under the crowdsensing concept. It makes use of the pervasive presence of mobile devices, such as smartphones and tablets, with built-in inertial sensors and positioning and communication capabilities that can transform vehicles and passengers into mobile sensing agents.

Concerning inertial-based methods in railroad monitoring, the primary problems are related to the high vibration acting on sensors installed on the axle box [25], requiring more constant maintenance on sensors and more resistant devices. On the other hand, when the sensors are placed under the influence of suspension, as proposed for the very-low-cost devices, the appropriate definition of filters and processing methods to obtain realistic track geometry or track quality indexes in scenarios with speed and vehicle variations is pivotal. Moreover, considering future crowdsourced systems and the collective use of these very low-cost sensors (i.e., multiple sensors on board the same vehicle in different positions), issues such as the influence on the measurements of the longitudinal or transversal sensor position aboard the vehicle and the improvement in accuracy when integrating multiples similar sensors in the same vehicle were not utterly addressed.

In this paper, the results of tests using multiples consumer-grade low-cost sensors are presented. Each apparatus comprises a combination of a micro-electrical-mechanical system (MEMS)-based Inertial Measurement Unit (IMU), a mini Global Positioning System (GPS) module, a single-board microcomputer to control sensors and store data in a dedicated system, and a battery for autonomous operation. Regarding the proposed tests, these devices are a more affordable and flexible option than smartphones, and their similarity in quality level allows for extrapolation of the conclusions to a collaborative smartphone-based system. Nine of these devices were attached to the track inspection trains of the Italian Railway Network and tested in different spatial configurations over four days of travel throughout the Italian high-speed network.

This work presents two main analyses: a) comfort assessment by calculating vertical frequency-weighted accelerations in accordance with ISO 2631 (standard for evaluation of human exposure to whole-body vibration), with comparison among sensors and analysis of improvement given by data fusion; and b) validation of the results considering reference data from the inspection train for one of the selected stretches. Besides the comfort analyses themselves, the proposed method allows for an indirect track quality assessment. As the main contribution, this work aims aim develop the basis for the collective track monitoring, dealing with issues such as the magnitude of influence of sensor position inside train cabins and the accuracy improvement when integrating data from different devices. Moreover, the device developed in this research is a relevant contribution as a possible dedicated low-cost tool for track monitoring.

2 Background and related work

2.1 Vehicle response to the track features

The response-based track inspection principle has been used since the first track recording vehicles [26] and considers the relationship between vehicle displacements and railroad geometry features and irregularities. Rail vehicle excitation occurs at the wheel-rail interface, and the associated contact forces are nonlinear functions of variations of lateral and vertical track position and speed [27]. Besides track geometry, irregularities, and velocity, other aspects such as track stiffness, vibration isolation given by suspension, vehicle body features, and relative distance to

bogie centreline also influence the amplitude of the irregularity-related linear and angular displacements inside the car body [24,27,28].

Direct track geometry assessment can be performed using accelerometers installed on axle boxes, applying double integration on the acceleration data acquired, in a simplified approach [3,25] or ideally considering the rail-wheel contact modelling in the transfer function [18,29–31] to estimate irregularities. Accelerometers installed on the bogie and inside the car body are widely used for running behaviour and ride comfort assessment [3,7,32]; at any rate, they also can be used for geometry analysis if the suspension displacements are known [4] or if the dynamic properties and the operating conditions are well known [33,34] and considered in the train-track dynamic model. To meet the data quality requirements, the use of tactical, industrial or navigation-grade inertial sensors (medium/high-cost) in such systems is preferred. Moreover, the georeferencing of track data is usually performed through GPS coordinates (often with differential correction) integrated with signalling information, odometry and inertial data.

An alternative approach is the analysis of vehicle vibration in terms of its expected spectral response to irregularities. In this approach, while track designed geometry can be mainly regarded as long-wavelength features, the deviations in geometry (irregularities) and the rail wear are described according to their typical wavelength ranges. Thus, the wheelset will be subjected to an exciting frequency f under the fundamental relationship $f = v/L$ [35–37], where L is the considered irregularity wavelength modelled as sinusoidal function on which the train is running.

For the sake of human sensitiveness, passenger coach suspension is usually designed to isolate the cabin for frequencies above about 2 Hz [38]. Moreover, there are the vibration transmission attenuation or amplification depending on the proximity of the excitation frequency to the natural frequency [28,38], being the resonance frequency of the sprung mass above the secondary suspension ranges is about 0.5-1 Hz for the main vibration modes [35,39] and 8-10 Hz for bending [27,40]. The former frequency range prevails above the bogies, while the latter prevails at the centre of the car body [40].

From [7,35,37,41], typical wavelengths associated with some of the main track aspects can be described as presented in Table 1.

Table 1. Main track aspects and their corresponding wavelengths [7,35,37,41]

Wavelength range [m]	Track aspect
0.03–0.06	Very short wavelength rail corrugation, rail joints, small size squats
0.06–0.25	Short wavelength rail corrugation, medium size squats
0.25–0.60	Medium wavelength rail corrugation, large size squats, turnout frog
0.60-0.70	Sleeper spacing
0.60–2	Long-wavelength rail corrugation
0.60–2	Ballast fouling
3-25	European Committee for Standardization (CEN) wavelength range D1 for longitudinal level and vertical alignment (short wavelength)
25-70	CEN wavelength range D2 for longitudinal level and vertical alignment (medium wavelength)
70-200	CEN wavelength range D3 for longitudinal level [70-150m] and vertical alignment [70- 200 m] (long wavelength)

Irregularity-related lateral and vertical signals obtained may be simplified by the sum of multiples irregularity-related signatures, each of them approximated by a sinusoid. This spectral aspect enables Fourier Transform and wavelet-based analyses of responses to extract track features from vibration signals. On the other hand, the longitudinal vibration component associated with track irregularities is usually less relevant than its orthogonal counterparts. Regarding longitudinal models [42,43], it can be considered that this component is mainly due to coupler impact transients

as an indirect effect of irregularity on adjacent coaches. In addition, this component is marginal when compared to the longitudinal travelling acceleration [44].

As discussed in the European railway standards [41,45] considering the well-known theoretical consideration on the vehicle-track model and the practical experience, there are clear relationships between the dynamic quantities measured on each car body axis and the different track geometry parameters. Thus, the predominant influences on car body response are described as follows:

- Vertical accelerations in the car body are mainly due to defects in longitudinal level.
- Lateral accelerations are mainly affected by track alignment and twist/cross level.

However, the relative motion between the wheelset and the track results that the lateral displacements do not fully follow the lateral irregularities [46,47], which may reduce the correlation between lateral irregularities and train cabin lateral accelerations.

A practical issue regarding sensors positioned in the cabin is the influence of sensor position on signals. If a sensor is placed right over one of the sides of a given bogie, it is expected to follow more closely the track irregularities of this side. When displaced away from this bogie, the influence of the other bogies increases, and the signal presents a distinct form due to phase shifts and differences in magnitude. For example, considering an accelerometer over the rear bogie and another one over the front bogie on the same side, they will be in phase for bounce mode responses and out of phase for pitch mode responses [4]. Regarding magnitude, acceleration at coach extremities is expected to be more significant than at the body centre [40,48]. On the other hand, tendencies of vibration variation from the front to the rear coach of the train set are intricate and depend on factors such as the suspension parameters (mean value and variation between coaches), the equivalent conicity, the stiffness and damping coefficients of coaches coupling, the speed, the train length and the mass variation between coaches [40,48,49].

Another practical issue is the Nyquist sampling theorem, which states that a signal with a given bandwidth f_0 can only be reconstructed from its sample values if the sampling frequency is over twice its bandwidth f_0. [50]. From this theorem, the Nyquist sample rate $f_N = 2f_0$ is the minimum sample rate $2f_S$ for a proper signal characterisation without aliasing. Moreover, the f_0 frequency defines the low-pass filter's minimum cut-off frequency applied as an antialiasing filter when sampling [51]. Adopting a reverse calculation, the minimum monitorable track irregularity λ for a fixed sample rate depends on the running speed v and is given by $v / 2f_S$.

Using some of the above-discussed characteristics, low and very low-cost inertial sensors have been the basis for many affordable experimental alternatives for track quality monitoring. These initiatives vary concerning the following main aspects:

- Sensor location, i.e., whether in the axle box [9–14], bogie [15–18], or car body [19–22].
- Sensor grade: relative low-cost, comprising tactical, industrial, and automotive-grade accelerometers [9,11–13,18,19], and very low-cost, comprising consumer-grade sensors (smartphones and similar) [20,21,23,24,52].
- Signal processing approach, i.e., whether track profile is explicitly estimated by using detailed knowledge of the vehicle dynamic model and its parameters [31,53–55], or it is implicitly evaluated based on the effect of track irregularities on vehicle vibrations, considering signal-derived features in time or frequency domain [9,15,35,56,57], or indexes related to comfort [19] or safety [58].

2.2 Use of very low-cost inertial sensor in rail track monitoring

[25] highlighted the noise levels and poor stability of consumer-grade sensors, similar to those proposed in the present paper, as restrictions for their use in track profile direct reconstitution. Dealing with these limitations and those due to suspension influence, [59] presented a solution based on an Arduino microcontroller and a consumer-grade IMU composed of accelerometer and

gyroscope, which as applied on track misalignment identification through acceleration peaks and frequency spectrum over time analysis. [21] employed inertial sensors (accelerometer, gyroscope, and magnetometer) of eight smartphones attached to the car body of a track recording car to characterise track cant, curvature, and twist. These authors applied discrete wavelet transform and sub band coding algorithm to extract long and short wavelength features and yield results that were compatible with measurements of the state-of-the-art technique.

[20] obtained a good correlation between the standard deviation of vibration gathered by a smartphone installed on the cabin floor and standard deviation track longitudinal level in D1 and D2 ranges, enabling characterisation of structural performance and degradation in geometry. Based on the road impact factor, a track quality index based on the average g-force per unit of distance, [52] dealt with the inaccuracy of GPS from smartphones (in position and speed) and the non-uniform sampling and proposed a windowed averaging of impact factors calculated from successive train traversals.

2.3 Comfort analysis in railways and its relationship with track features

Concerning the ISO 2631-based approach, its concepts have been used in rail transportation to relate comfort perception (combination of track irregularity and vehicle characteristics) with track features or quality parameters [19], in an indirect method to analyse the track quality, characterise the passenger comfort in accordance with ISO 2631 standard using an accelerometer installed on the floor of a subway train. With this approach and its geovisualization, multiple transversals exhibited a consistent correlation between high frequency-weighted vertical acceleration and the presence of switches. [60] created a smartphone application for comfort analysis and tested it on two devices. The authors applied an artificial neural network using data gathered by a more accurate piezoelectric accelerometer for training, and comparison between this technique output and track geometry parameters was recommended as further work.

[61] developed a smartphone-based track and ride monitoring application that registers the perception of ride comfort in the cabin according to ISO 2631 and its relation with track features such as switches, crossings, track stiffness variations, and deteriorated turnouts. [23] performed a similar ISO-based analysis employing smartphones and concluding by the association between discomfort peaks and track stiffness transition zones.

3 Materials and Methods

In this research, the two main aspects tested within the proposed collective monitoring system are: a) the use of consumer-grade (i.e., smartphone-grade) sensors; and b) the use of trains that are similar to usual passenger trains in terms of the number of coaches, ideally train recording vehicles that can provide reference data for further validation. The material and methods adopted to meet these ideas and the proposed data processing methodology are described as follows.

3.1 Device description

The concept of a low-cost collective monitoring system is related to the crowdsensing idea and the use of smartphones sensors to describe vehicle vibrations and, consequently, enable track quality estimation. Therefore, viability tests for this monitoring tool consider the use of multiple sensors operating in parallel during the same train trip. The basic hypothesis considers that a set of low-quality sensors can, in a combined way, offer a robust and accurate operation by minimising the variance fluctuation of individual sensors. Since the acquisition and use of smartphones present drawbacks such as cost of acquisition, power limitations, and restrictions on changing and handling proprietary hardware/software components, the option was to construct dedicated devices using sensors similar to smartphone-grade sensors to emulate these gadgets affordably. Moreover, these devices themselves are regarded as possible very low-cost, easy-to-operate tools for track quality monitoring, working together with traditional techniques or operating in a sensing system together with smartphones and tablets.

Nine devices were developed based on these concepts, with each device composed of the following components (as described in a previous work that considered their use on road monitoring) [62]:

- Raspberry Pi Zero W, a low-cost single-board microcomputer with a 16 GB micro-SD for Raspbian (Raspberry operating system) installation and data storage. The device has an 802.11 wireless LAN (Wi-Fi) and a Bluetooth interfaces, facilitating the communication to set up the devices before trips and the parallel control during the experimental tests.
- InvenSense MPU-9250, a MEMS-based Inertial Measurement Unit (IMU) with10 degrees-of-freedom. Besides the three-axis inertial sensors (accelerometer and gyroscope), this model features a three-axis magnetometer and a pressure module BMP280 [63,64].
- U-blox mini GPS module, NEO-6M model [65]. This receiver model performs single-point positioning using the C/A code transmitted on the L1 frequency by the GPS constellation.
- Portable charger with 10,400 mAh capacity as energy supply.

GPS and IMU data were acquired and handled under two tools: the C++/Python library RTIMULib [66] was employed for the essential tasks involving MPU-9250 data gathering, namely sensors setup, initial calibration, and conversion of output values from hexadecimal to floating-point representation. Besides raw measurements, this library yields attitude (roll, pitch, and yaw, in degrees) estimation from accelerometer, gyroscope and magnetometer integration using Extended Kalman Filter. Considering the GPS module, the Python library GPSD [67] was used for the setup and the acquisition of position, velocity, and time (PVT) data using the United States National Marine Electronics Association (NMEA) protocol.

Preliminary tests using mid-level smartphones running Android (Samsung GalaxyA30, Lenovo Vibe K5, and Samsung Galaxy J2 models) showed that the maximum stable sample rate was about 100 Hz for inertial data and 1 Hz for the GPS data (this being the maximum rate for these models). Thus, regarding optimum processing and storage performance, the vibration behaviour of the car body, and the usual sample rate for mid-level smartphones, the output data rate was set up at 100 Hz for inertial data and 1 Hz for the GPS data. Nevertheless, although maintaining 100 Hz for inertial data during the first ten seconds of operation, the actual mean sample rate was about 83 Hz, probably due to hardware and software limitations. Furthermore, a full-scale range of ± 2g was adopted for the accelerometer considering the typical values for smartphones, suitability to expected maximum accelerations in train cabin (less than 1g disregarding gravity) [2,68], the trade-off between range and sensitivity, and the exposure to significant non-linearity errors when operating near the limits of the range.

GPS and IMU data are recorded in separate files since this configuration presented the most consistent performance during the preliminary tests. Given the lower rate compared to the IMU and the separated files, interpolation of PVT data using the operating system timestamp as the key attribute is necessary. Another relevant aspect is that the device presented an autonomy of about 50 hours under the aforementioned configuration.

3.2 Experimental tests within a track recording train

The other central aspect of the collective concept is the use of in-service vehicles. This conditions how the test should be carried out, preferentially using diagnostic trains that are physically similar to commercial trains in terms of the number of coaches and can yield dynamic and geometric data as ground truth for further analyses. Thus, the experimental tests were performed on board the diagnostic train ETR500Y2 (Figure 1), owned by the Italian Railway Infrastructure Manager (*Rete Ferroviaria Italiana*, RFI) and is adapted from an ETR500 train model used exclusively on the high-speed network.

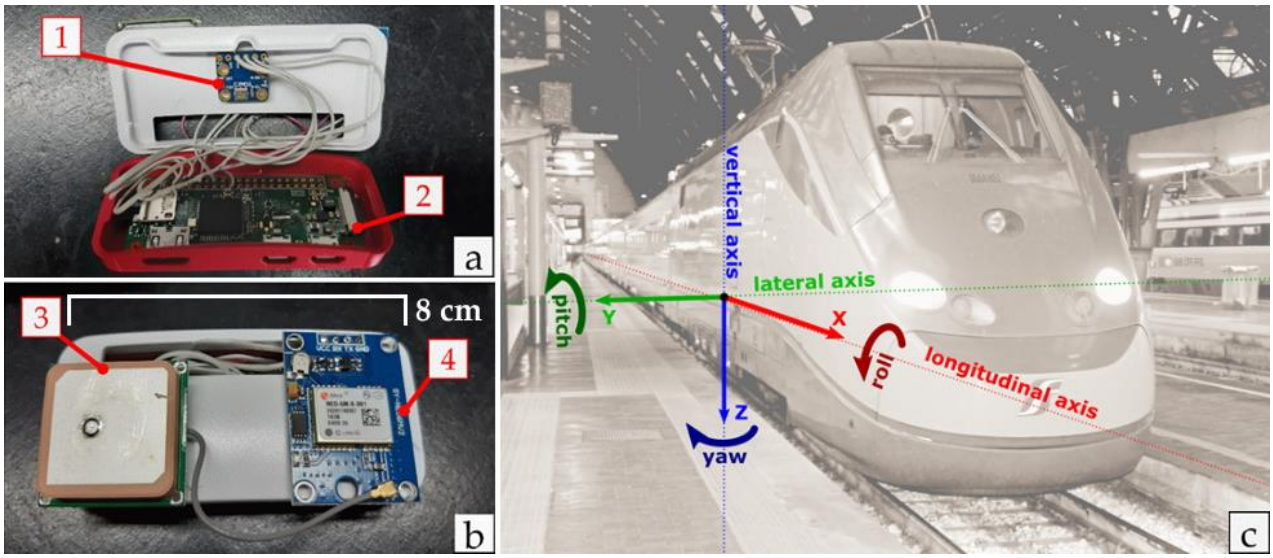

Figure 1. The developed device and the train used in the tests: (a) internal view of the device showing the IMU module (1) internally glued to the case and the Raspberry Pi Zero W (2); (b) external view highlighting the GPS antenna (3) and the u-Blox GPS module glued to the case; (c) the *Diamante* train and the axes orientation for the tests

This train, also known as *Treno Diamante* (an acronym for *Diagnostica e Manutenzione Tecnologica*), consists of two locomotives (one at each extremity) and eight two-bogie trailer coaches, carrying more than 200 onboard sensors for the inspection of track, energy system, signalling, telecommunication and ride dynamics [7,69,70]. The running dynamic characterisation comprises lateral and vertical acceleration monitoring in the axle box, the bogie, and the train cabin by 12 high-grade mono-axial MEMS accelerometers, which operate at 1 kHz and are distributed over the coach dedicated to this purpose. Moreover, laser-based systems and inertial platforms are employed for track geometry recording, surveying the track irregularity parameters described in Table 2.

Table 2. Track irregularity parameters surveyed by *Treno Diamante* and their features [7]

Parameter	Measurement technology	Chord length	Spatial resolution	Measurement uncertainty (2 σ)
Longitudinal level – right/left (range D1: 3-25 m)	Optical laser	23.220 m	0.5 m	± 1 mm
Longitudinal level – right/left (range D2: 25-70 m)	Optical laser	23.220 m	0.5 m	± 3 mm
Longitudinal level – right/left (range D3: 70-150 m)	Optical laser	23.220 m	0.5 m	± 5 mm
Alignment - right/left (range D1: 25-70 m)	Optical laser	23.220 m	0.5 m	± 1.5 mm
Alignment - right/left (range D2: 25-70 m)	Optical laser	23.220 m	0.5 m	± 4 mm
Alignment - right/left (range D3: 70-200 m)	Optical laser	23.220 m	0.5 m	± 10 mm
Twist	Optical laser + inertial platform	3.000 m and 9.000 m	0.5 m	± 1.5 mm
Cross level	Inertial platform	-	1 mm	± 5 mm
Gauge	Optical laser	-	0.5 mm	± 1 mm

The *Diamante* system also outputs the longitudinal level (LL) and alignment (A) on a 10-metres chord. Moreover, combinations and derived parameters are also calculated on board or offline and delivered by the RFI system, namely:

- LL and A standard deviations for D1 (combining right and left) within 200 metres sections.
- From raw cross level, the system also outputs the cross-level deviation within a 10-m window and the superelevation deviation (difference between design superelevation and cross level)

Diamante's position data is obtained from a Differential GPS receiver and an odometer. The train performs a 5-days inspection throughout the Italian high-speed, high-capacity network every two weeks and can operate at speeds up to 330 km/h (compatible with maximum commercial speeds of about 300 km/h).

This paper describes the results of the experimental tests performed from 14th to 17th January 2020 through the Italian high-speed, high-capacity rail network. It comprises two corridors: Milan-Salerno and Turin-Venezia (excluding the future high-speed stretch between Padua and Brescia). For the sake of logistic restrictions, tests were carried out only during the last four days of the 5-days inspection work, which itineraries are presented in Table 3. The considered track has a gauge of 1435 mm (international gauge), maximum design speed varying from 200 to 300 km/h depending on the stretch and varies between ballasted and slab track stretches.

Table 3. Itinerary of the tests performed within the Diamante train through the Italian rail network.

Test day	Date	Origin	Intermediary stops	Destination	Approx. length (km)
#1	Jan 14th 2020	Naples	Rome > Florence > Bologna	Milan	800
#2	Jan 15th 2020	Milan	Turin > Brescia > Milan > Brescia	Vicenza	640
#3	Jan 16th 2020	Vicenza	Venice > Padua > Venice	Milan	410
#4	Jan 17th 2020	Milan	Bologna > Florence > Rome	Naples	800

The sensors were directly attached to the train floor using a double-sided adhesive tape. As illustrated in Figure 1, the IMU x-axis was aligned to the vehicle longitudinal axis, while the y-axis was aligned to the lateral axis and the z-axis to the vertical axis in the vehicle frame. Moreover, to enable analyses regarding the influence of the sensors positions on measurements, we adopted a different sensors distribution inside the train for each day test. These distributions, depicted in Figure 2, are described as follows:

- **Day #1**. The nine sensor sets were installed at the same approximate point. They are distributed over an area of 0.3 m x 0.5 m. The sensors were attached to the car floor under the ninth right window in the eighth coach (right over the rear bogie).
- **Day #2**. The nine sensors were distributed along the eighth coach under each of the ninth window. Since the distance between bogies is about 19 m, the distance between two consecutive sensors is about 1.9 m.
- **Day #3**. We installed a sensor in each coach at homologue positions: under the ninth right window in the given coach (right over the rear bogie). The distance between two consecutive sensors is equal to the coach length: 26.1 m.
- **Day #4**. The nine sensors were distributed along the same transversal section (2.8 m) aligned with the ninth right window in the eighth coach. To not obstruct RFI staff's passage, eight sensors were equally spaced along the right half of the transversal section (1.4 m), while the ninth sensor was installed at the left extremity of this section.

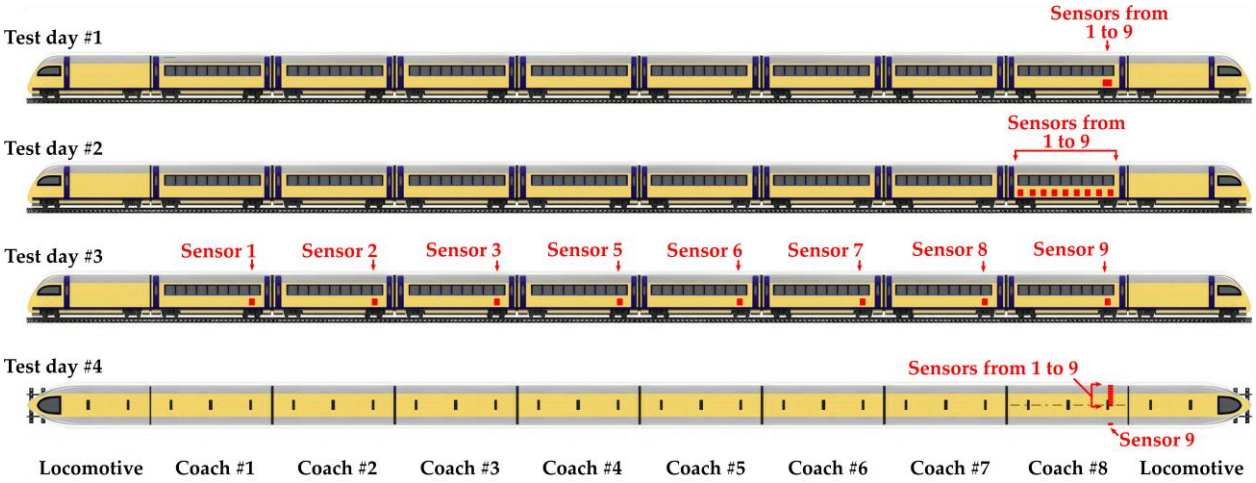

Figure 2. Formation of the *Diamante* train and the sensors distributions for the four test days.

The analysis considers only trip intervals in which the trains travelled at a quasi-constant speed to eliminate the influence of speed variation on measurements. The Augmented Dickey-Fuller test (ADF) [71] was applied for these trip intervals, and the hypothesis of non-stationary was rejected at a significance level of 1%. Table 3 shows the selected trip intervals for statistical comparison, which are also regarded as road sections in the space domain.

Table 4. Trip intervals/road stretches selected for the proposed analyses

Test day	Stretch	Start time (s)	End time (s)	Length (m)	Average speed (m/s)	Std. deviation speed (m/s)	Approximate location	Train direction
#1	A	8400	8600	13260	66.3	0.7	Montepulciano	Forwards
#1	B	13200	13500	20090	67.0	1.6	Modena	Forwards
#2	A	4600	5250	53940	83.0	0.7	Novara	Forwards
#2	B	18100	18380	15180	54.2	1.4	Milano	Forwards
#3	A	6710	6940	13961	60.7	1.6	Padova	Backwards
#3	B	23200	23430	10189	44.3	0.7	Soave	Forwards
#4	A	9850	10050	10080	50.4	1.0	Parma	Backwards
#4	B	23200	24300	73191	66.5	0.8	Arezzo	Backwards

3.3 IMU measurement model

To characterise the measurable quantities using the proposed devices, a basic model of the inertial measurements based on vehicle kinematics is built considering the influence of track geometry and irregularities on perceived accelerations in the train cabin. Based on elements presented in previous works (cited as follows) and considering the vehicle-track behaviour discussed in Section 2, the simplified acceleration vector $\boldsymbol{a}$ perceived in the sensor frame *s* attached to the train cabin is obtained as:

$$\boldsymbol{a}^{s} = \boldsymbol{g}^{s} + \boldsymbol{c}^{s} + \boldsymbol{t}^{s} + \boldsymbol{n}^{s} + \boldsymbol{b}^{s} + \mu^{s} =$$

$$\begin{bmatrix} -g\ sin\ \theta \\ g\ cos\ \theta\ sin\ \varphi \\ g\ cos\ \theta\ cos\ \varphi \end{bmatrix}^{s} + \begin{bmatrix} \dot{v} \\ c_H\ v^2 \cos\gamma - c_V\ v^2 \cos\gamma \\ c_H\ v \sin\gamma - c_V\ v^2 \cos\gamma \end{bmatrix}^{s} + \begin{bmatrix} i_X \\ i_Y \\ i_Z \end{bmatrix}^{s} + \boldsymbol{n}^{s} + \boldsymbol{b}^{s} + \mu^{s}, \quad (1)$$

where:

- **g** is the gravity component in the sensor frame using the XYZ rotation sequence applied to the gravity vector [72,73]. While g is the gravitational acceleration, θ is the vehicle pitch angle, and φ is the vehicle roll angle. Pitch and roll angles are measured in relation to the horizontal plane and are mainly associated, respectively, with the track slope and the cant angle plus the suspension effect on these angles (pitch and roll stiffnesses).

Complementary, high-frequency variations in these angles also depend on rolling and pitching car body vibration modes due to track irregularities.

- **c** is the kinematic component associated with vehicle displacement on the road regardless of deviations from design geometry. Whenever the vehicle is moving, the speed variation $\dot{v}$ is perceived in the x-direction. Concurrently, the horizontal (c_H) and the vertical (c_V) curvatures produce a centrifugal acceleration in the vehicle frame given by the relation c·v, where v is the vehicle speed. In addition, the centrifugal accelerations are decomposed according to the roll angle γ [73].
- **t** is the track irregularity component. Regarding the x and y axes, components can be regarded as the sums i_Y and i_Z of multiples irregularity-related sinusoidal signatures. The component i_X is different in form and considerably less significant than their orthogonal counterparts.
- **n** is the background vibration due to the traction motor vibration, the auxiliary power system and the heating, ventilation, and air conditioning (HVAC) system [4,74]. For the considered trailer coaches, there is not component due to the traction motor. Furthermore, for the considered tests, the preliminary analysis of the signals for intervals with stationary train demonstrated the absence of relevant vibration components due to the other subsystems. Thus, this component will be ignored in further considerations.
- **b** is the slowly time-varying sensor bias [73,75].
- **μ** is the sensor noise [73,75].

Under this model and considering a quasi-constant speed during the selected stretches, the different arrangements adopted in the tests can be read according to the following aspect:

- **Day 1**: sensors yield similar data in terms of **g**, **c**, and **t** since they are in the approximately same position. There are differences among them in terms of **b** even after the calibration (eventual thermal, mechanical, and electrical variations among the sensors) and **μ** (stochastic nature of noise) [76].
- **Day 2**: sensors yield similar data in terms of **g** and **c** (coach as a whole perceiving approximately the same pitch and roll angles and the same curvatures) and different data in terms of **t** (phase shifts and differences in amplitude due to distance to bogies centrelines), **b,** and **μ**.
- **Day 3**: sensors yield signals with similar shape in terms of **t**, with expected magnitude variations due to suspension parameters variation from one car to another and expected train set dynamics (higher vibration in the last cars). The signals are also similar in terms of **g** and **c**, with discrepancies in magnitude due to possible differences in roll and pitch coefficients. For these three components, there is a phase shift proportional to the distance among sensors. Moreover, they produce different data in terms of **b** and **μ**.
- **Day 4**: sensors yield similar data in terms of **g** and **c**, and different data in terms of **b** and **μ**. Regarding **t**, variation in transversal position results in major or minor influence of a specific track side.

It is noteworthy that bias can be reasonably handled as a constant within the eight selected intervals with slow variation during the trips. Thus, offset error can be estimated and corrected considering accelerometer readings during trip intervals in which the sensor is motionless and horizontal. However, offset is not critical for frequency-weighted accelerations since it is perceived as a long-wavelength feature outside the comfort frequency boundaries. Furthermore, sensor lateral distance to track centreline in curves results in negligible discrepancy in centrifugal accelerations.

3.4 Data processing

Firstly, for each sensor, GPS data were linearly interpolated at IMU updates intervals between two consecutive GPS updates (1 s interval), which yields a maximum error of about 0.15 m in the worst

case. Moreover, the chainage is calculated as the horizontal travelled distance incrementally calculated from the stretch starting point. For this task, the geographic coordinates (WGS84 datum) were transformed to projected coordinates (UTM Zones 32N and 33N, WGS84 datum).

3.4.1 Time-lagged cross-correlation

The main goals of the described analyses are the comparison among sensors in different experimental arrangements and the comparison of them with reference data. Since there are possible synchronisation errors and phase shifts due to the differences in position among the sensors, the similarity between two signals in the time domain is measured through time-lagged cross-correlation [50,77]. The normalised linear cross-correlation coefficient r between two signals x and y with N samples is defined as:

$$r = \frac{\sum_1^N (x_i - \bar{x}).(y_{i+L} - \bar{y})}{\sqrt{\left[\sum_1^N (xi - \bar{x})^2\right]\left[\sum_1^N (yi - \bar{y})^2\right]}} \quad (2)$$

where $\bar{x}$ and $\bar{y}$ are the mean values of x and y, respectively, and L is the lag between the signals. The numerator is the cross-correlation function, while the denominator performs its normalisation by the standard deviation of both series. For each pair of signals from the same trip, the time-lagged cross-correlation algorithm calculates r for L varying within a sample window and searches for the maximum r and the associated lag. This lag is assumed to be due to the synchronisation errors and the differential position between sensors.

3.4.2 Data fusion

Firstly, the n different signals were resampled to a common and equally spaced time vector. Afterwards, the fusion of the multiple sensors operation simultaneously considered two main aspects to obtain a combined (or mean) signal:

- Spatio-temporal alignment of the signals. Besides the GPS time-based synchronisation correction and the data georeferencing for each sensor, the lag from time-lagged cross-correlation results for each axis is applied to maximise correlation among signals. This approach is usual for signal alignment [50]. Since only intervals with quasi-constant speed are considered, this match can be done in the time or space domain with the remotion of lags obtained for each axis.

- Combination of the signals by using the mean calculation., and the mean signal is calculated. Considering a scenario where sensors are redundant and measurements present approximately the same variance, there is a theoretical decrease of noise (or variability of the mean) when averaging N independent measurements by a $1/\sqrt{N}$ factor under Central Limit Theorem (CLT) [72,78].

This combination is firstly done for the roll and pitch estimates (section 3.4.3) to provide a unified inclination estimation. From this result and the subsequent gravity compensation, the combination process is also done for the compensated acceleration to obtain a unified acceleration signal on a signal level fusion process. In parallel with this process, comfort analysis using the individual signals is performed, and the mean comfort indexes are calculated at the end, i.e., on a feature level fusion process. This alternative process emphasises how the mean signal reduces noise impact on results in contrast to the mean index.

3.4.3 Gravity compensation

In order to compensate gravity components from measurements, roll and pitch estimates are required. Due to noise and bias instability associated with gyroscope, the simple integration of angular velocities to estimate roll and pitch angles results in an angular random walk. On the other hand, acceleration-based inclination estimations do not present drift but are unusable whenever the monitored object experiences sustained accelerations, such as the centrifugal acceleration in

curves. In these cases, the residual acceleration may indicate an inclination opposite to the real track bank, a behaviour verified with the RTIMULib estimations from accelerometer-gyroscope fusion).

Since the present approach considers the collective use of sensors, we propose a simplified way to estimate angles considering the fused response of the sensor population. For roll angle, the first step is the numerical integration of the angular speed combination (mean signal) around the x-axis. This integration can be done for small inclination angles (ruled by the small slope and cant rail track angles) since the angular speed ω in the sensor frame can be considered approximately equal to the angular speed in the navigation frame. The second step is the random-walk effect correction regarding track constraints: when travelling on a tangent, the roll angle must be about 0°. Under this concept, integration drift is estimated through the best fitting line for considering only tangent sections and the remotion of this value, enforcing an angle about 0° on these sections. Thus, the i_{th} roll value (φ_i) at the instant t_i is given by:

$$\varphi_i = \varphi_{i-1} + \int_{t_{i-1}}^{t_i} \omega_X(t)dt - y(t_i) \quad (4)$$

where $\omega_X(t)$ is the angular speed around the x-axis and y(t) is the best fitting linear function for tangent sections.

In addition, pitch estimation is done through a complementary filter (alpha = 0.98) combining angular speed signals for high-frequency variations and inclination from combined barometer heights for low-frequency variation, once again using the mean signal from the sensor population. Barometric height is obtained from RTIMULib height output, which approximately follows the datasheet relationship of ± 0.12 hPa for ± 1 m and the conventional barometric formula considering a constant temperature. Variations in temperature impact absolute values but does not affect the height variations approximation. In the end, an additional correction step is necessary to identify and eliminate data linked to pressure transient (i.e., when crossing a tunnel), once again using track constraint: inclination derived from barometer should not be greater than the maximum slope angle (about 1.1°). Thus, i_{th} pitch value (θ_i) is given by:

$$\theta_i = (1 - 0.98).(gyr_i) + 0.98.(bar_i) =$$
$$(1 - 0.98).\left(\theta_{i-1} + \int_{t_{i-1}}^{t_i} \omega_Y(t)dt\right) + 0.98.\left(arctan\ \frac{h_i - h_{i-1}}{d_H}\right) \quad (5)$$

where gyr_i is the pitch estimation from angular speed $\omega_Y(t)$ and bar_i is the pitch estimation from the barometric height variation (h_i - h_{i-1}) and the horizontal distance d_H between i-1 and i calculated from GPS coordinates.

3.4.4 Frequency weighted accelerations according to the ISO 2631

The ISO 2631-1:1997 (Mechanical vibration and shock — Evaluation of human exposure to whole-body vibration) [68] was established by the International Organization for Standardization (ISO) to provide methods for whole-body vibration assessment regarding human health and comfort, vibration perception, and incidence of motion sickness. The standard comprises guidance on vibration measurement and evaluation using frequency weighted root-mean-square accelerations. Since one of his motivations is the comfort perception in vehicles, its parameters were used in the road [79–84] and rail transportation [19,23,24,85] to analyse merely comfort or to relate comfort perception (combination of track irregularity and vehicle characteristics) with track features or quality parameters.

The considered standard defines that vibration frequencies should be weighted according to human sensitivity for each frequency. Therefore, the acceleration signal is analysed through frequency-weighting of acceleration spectra, considering the frequency range of interest for the

human response to vibrations (from 0.5 to 80 Hz) and its respective 23 one-third octave bands, each of them with a specific weighting factor. Thus, the resultant frequency-weighted root-mean-square acceleration aw for a given axis is given by:

$$a_w = \sqrt{\sum_{i=1}^{23} (W_i \cdot a_i)^2} \quad (3)$$

where Wi is the recommended weighting factor for the i_{th} one-third octaves band and ai is the rms acceleration for the i_{th} one-third octaves band for the given axis. There are different frequency weighting curves depending on the application, position, and axis, reflecting the different ways vibration affects humans. W_k is the recommended curve for the z-direction and W_d for the x and y directions for the main comfort analysis. However, the curve W_b is recommended for comfort evaluation in rail vehicles. Figure 3 depicts these weighting curves, being remarkable the slight difference between W_k and W_b.

For the present work, as an algorithm mathematically equivalent to recommended by ISO 2631 (Eq. 3), the frequency weighting of acceleration spectra was performed through signal decomposing into each one-third octave band and the subsequent weighted sum of data of these bands, resulting in a weighted signal in the time domain [86,87]. For signal decomposing, Butterworth 6th order passband digital filters were applied under ISO 2631 specifications with forward and backward pass to curb phase shift. In the end, the root-mean-square of the weighted accelerations is calculated within segments with the given lengths of analysis: 20, 50, 100, 200, and 500 m. Besides the 200 meters length recommended by the European Standard and the Italian manuals [7,88] and the 500 m length adopted for some high-speed networks such as the Chinese one [89], other lengths were tested regarding coherence with the usual wavelengths of the monitorable track features.

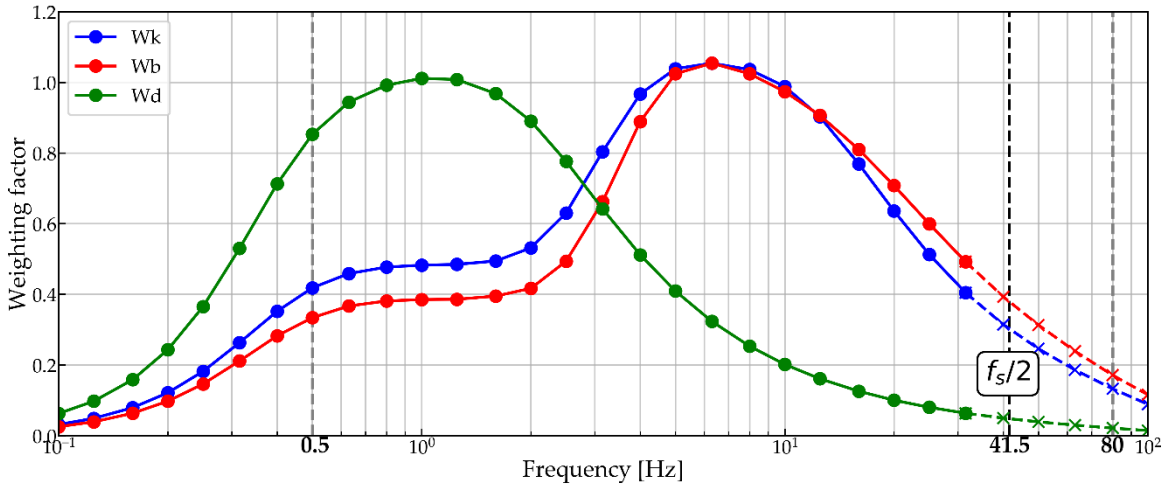

Figure 3. Weighting factors versus central frequency of each one-third octave band

The RMS values can be compared with the values indicated by ISO 2631 concerning the expected reaction to vibration in public transportation (Table 4). This standard emphasises that these values are not limits for accelerations but only approximations since other relevant factors need to be considered, such as exposure time, the activity performed when exposed to the vibration, acoustic noise, and temperature. This fact explains the superposition of the value ranges presented in Table 4.

Table 5. Likely reactions regarding comfort in public transportation

a_{WZ} values (m/s²)	Likely reaction
less than 0.315	Not uncomfortable
0.315-0.63	Little uncomfortable
0.5-1.0	Fairly uncomfortable
0.8-1.6	Uncomfortable
1.25-2.5	Very uncomfortable
more than 2	Extremely uncomfortable

Given the sample rate during tests (around 83 Hz), close to the usual maximum frequency sampling for average smartphones, only 19 of the 23 one-third octaves bands of interest (from 0.5 Hz to 80 Hz) can be analysed under the Nyquist theorem. However, the resulting inaccuracy is of small magnitude. Figure 5 depicts the weighting curves and highlights the non-analysable bands with cross markers and dashed lines, which shows that humans are less sensitive to vibrations over 10 Hz. Moreover, the more remarkable frequencies for high-speed lines are usually under 20 Hz [90], which is related to the fact that a passenger coach suspension aims to isolate the car body from frequencies above about 2 Hz [38].

Figure 4 presents the schematic flowchart of the analysis procedure applied for the present work.

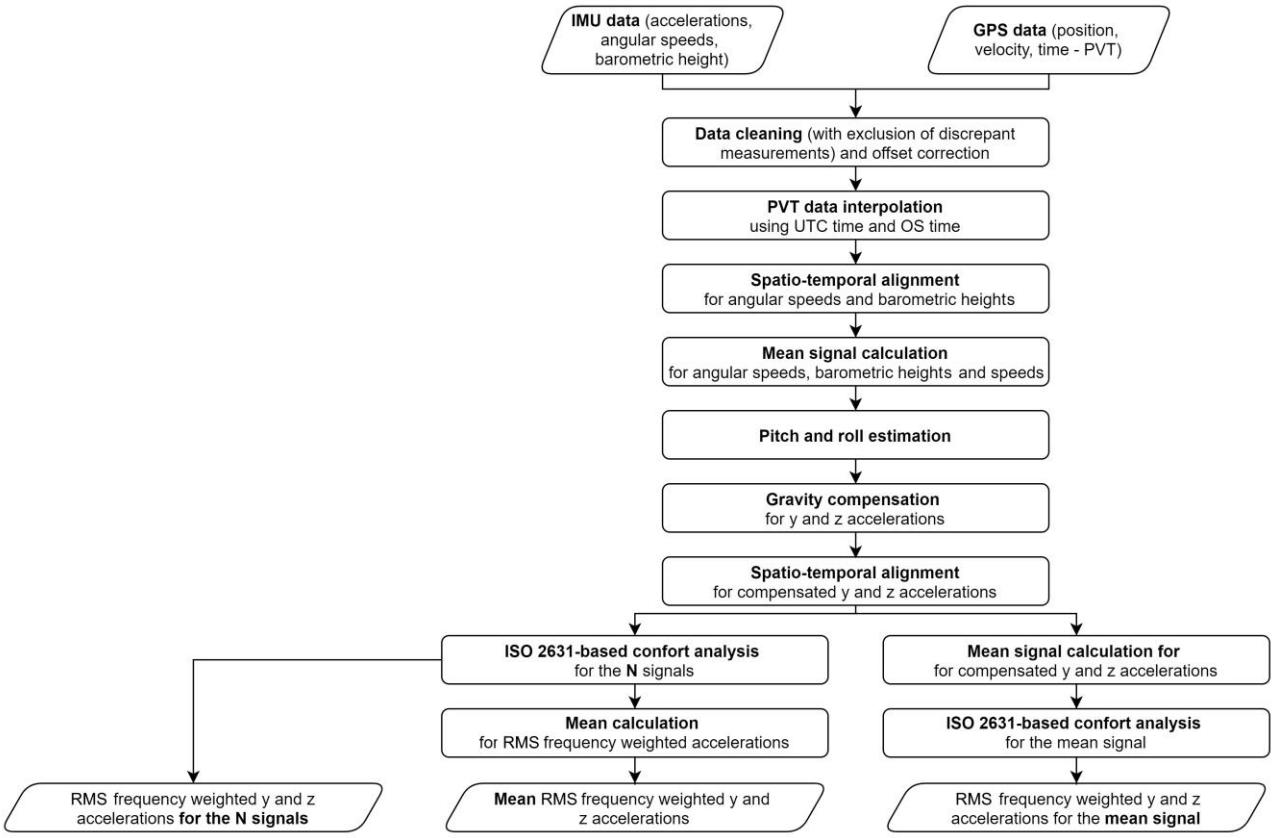

Figure 4. Schematic flowchart of the analysis procedure for data fusion and comfort assessment

3.4.5 Validation using *Treno Diamante* data

Furthermore, the comfort results are compared through correlation analysis with the standard deviation of the track parameters diagnosed by *Treno Diamante*. The discrete calculation (i.e., within segments of equal length) of the standard deviation as a track quality index is used in Italia, United Kingdom, Australia, and China [7,89,91].

Ideally, validation would consider all the selected stretches in all the considered sensors distributions. However, due to reference data unavailability issues for the present paper, it was possible only to perform analyses for the fourth day, stretch B.

4 Results and discussion

Firstly, the preliminary analysis and comparison among signals allowed for the identification of discrepant signals. It was identified that sensors 3 and 4 malfunctioned for all test days. Moreover, sensor 1 presented a discrepant behaviour during the second test day and was excluded from this day's analyses.

4.1 Roll and pitch estimation

The quality of the roll and pitch estimates is estimated through comparison with track angles obtained from reference data. It is known that these angles are mainly conditioned by cant and slope angles plus the suspension influence. Regarding roll, this influence is described by a roll coefficient that correlates vehicle body roll angle. Thus, the comparison between calculated inclination and track angles obtained from reference data provides a measure of estimation quality.

The proposed accelerometer-free algorithms yielded promising results, being the calculated roll and pitch vehicle angles highly correlated with, respectively, cant (r = 0.99) and slope (r = 0.86) angles for the validation stretch. Figure 5 illustrates the comparison between vehicle roll and track cant angles, with differences in magnitude due to the suspension roll coefficient. In turn, Figure 6 depicts the comparison between vehicle pitch and track slope angles, as well as highlights the tunnel impact on pressure-based measurements, also presenting the pitch estimation without correction for pressure transients.

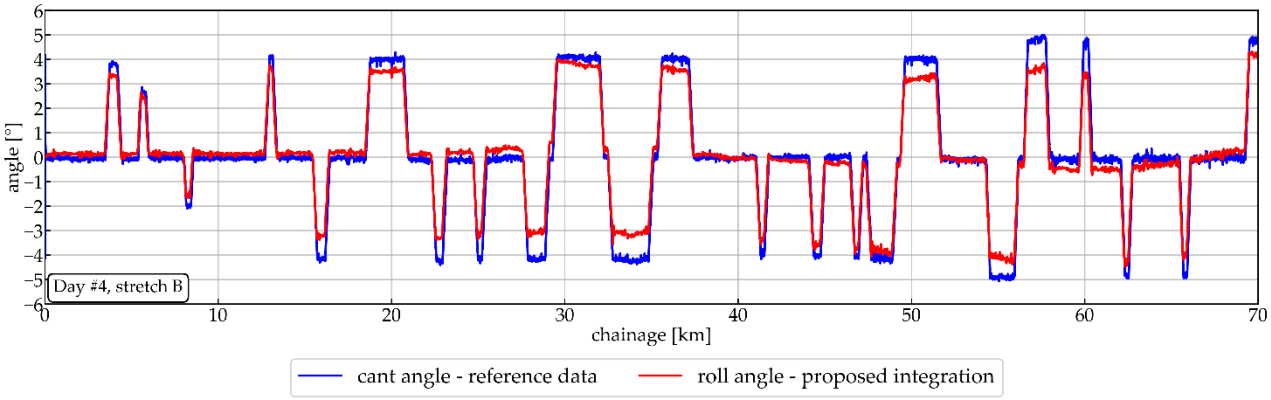

Figure 5. Roll angle estimate *vs.* reference track cant angle for 4th day, stretch B

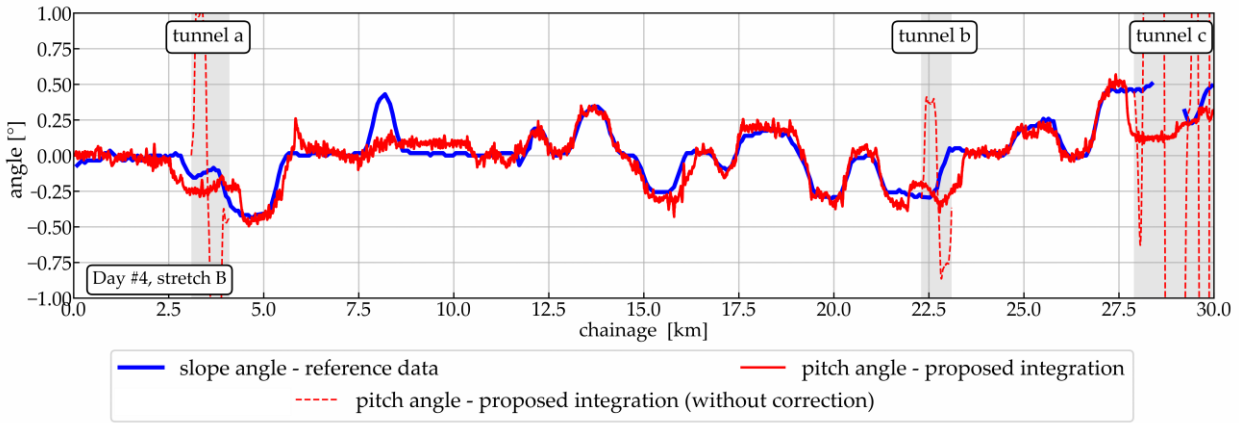

Figure 6. Pitch angle estimate *vs.* reference track slope angle for 4th day, stretch B

4.2 Comparison between individual and fused signals

Figures 7 and 8 depict, respectively, time and frequency domain (through Fast Fourier Transform) representations of the individual acceleration signals and the mean (fused) signal for the first day, stretch A. The first day was selected for this analysis because the sensors are theoretically redundant (under a similar solicitation), and the differences after offset correction are due only to the noise. This example is representative of the raw output obtained in other stretches and its relationship with the mean signal, which presents a notable smaller variance in amplitude that is convergent with the expected noise reduction. For this stretch, variance in the z-axis ranges from 0.06 to 0.14 m/s² and has a mean equal to 0.11, while the fused signal variance is equal to 0.04 m/s² (reduction factor of about $1/\sqrt{N}$ in relation to the mean, with N = 7 sensors). The same reduction factor is identified for the x-axis, while for the y-axis a smaller reduction factor is obtained due to the significant influence on variance of the high magnitude accelerations in a curve.

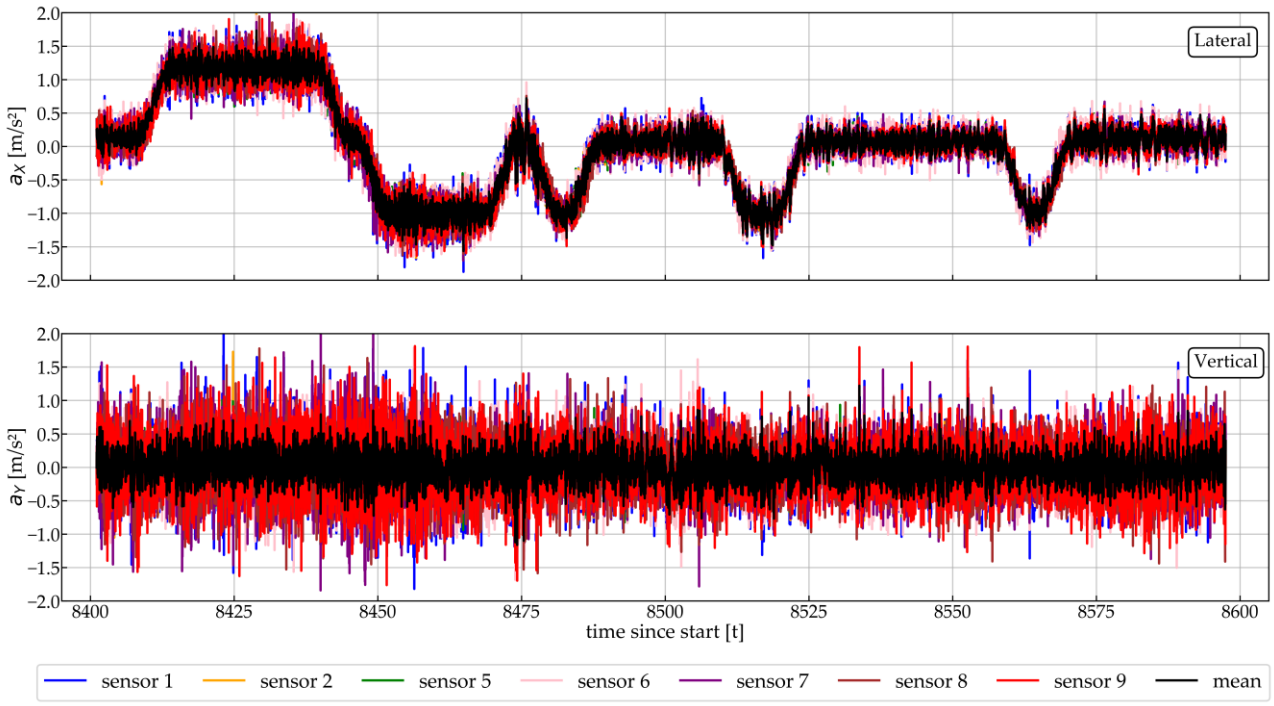

Figure 7. Individual and mean (fused) acceleration signals for the first day, stretch A

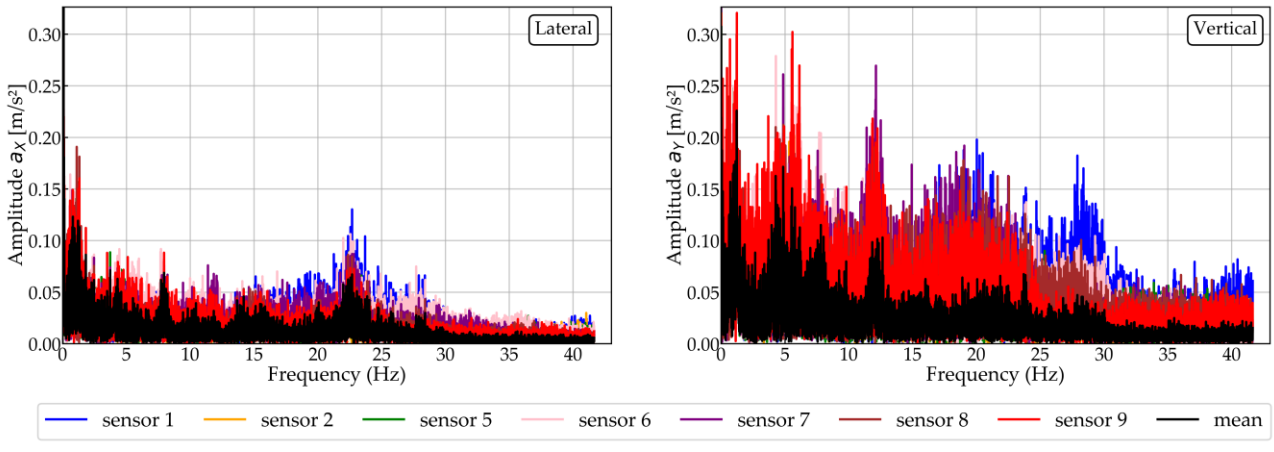

Figure 8. Frequency content of individual and mean (fused) acceleration signals for the first day, stretch A

4.3 Comfort analysis

The roll and pitch estimates were used to compensate the gravity from raw accelerations. To eliminate synchronisation errors, spatio-temporal alignment was enforced through time-lagged cross-correlation and lag correction for each axis. Afterwards, root mean square (RMS) frequency weighted accelerations in accordance with ISO 2631 were calculated for different sections lengths. Initially, Figures 9 and 10 compare the RMS frequency weighted results for different sections lengths considering the stretch B on the first day as a representative example. The vertical and horizontal scales for these graphs are the same to allow for magnitude comparisons.

Figure 9. Lateral RMS frequency weighted acceleration for different section lengths, section B on the first day

The natural result of lengthening the sections is the increase of the correlation between sensors due to peak attenuation. Another relevant aspect is the ever-smallest result for the mean signal due to noise reduction. It can be concluded that noise variation among sensors may influence the average a_W (represented by vertical shifts between the curves), but the general behaviour of its variation along the trip (i.e., form of the acceleration curves) is fairly preserved. When comparing the y and the x axes, it is also concluded that the expected smaller vibration in the lateral direction yields a greater concordance among the sensors.

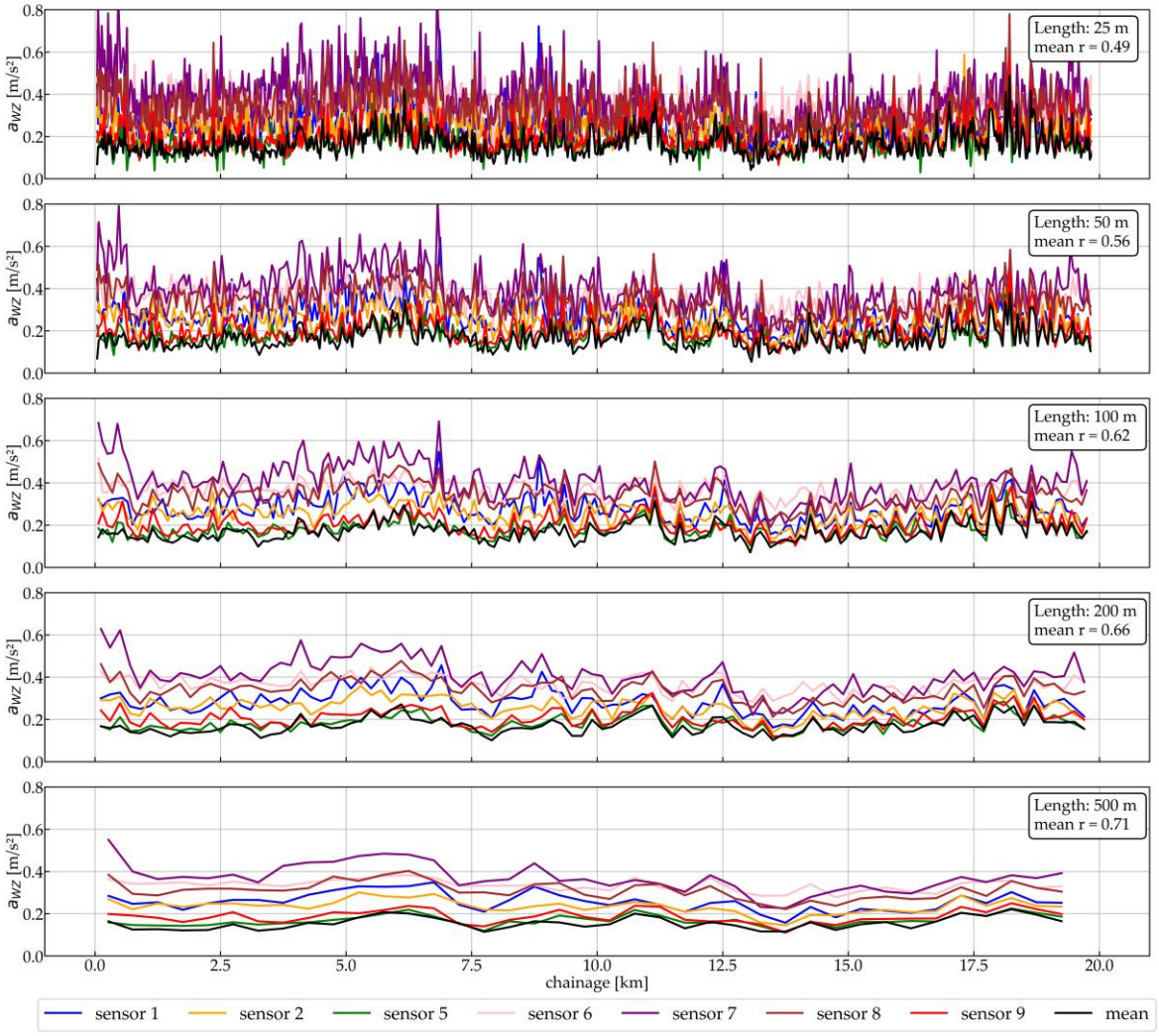

589

590 **Figure 10.** Vertical RMS frequency weighted acceleration for different section lengths, section B on
591 the first day

592 The following results are presented in terms of the 200-m section since this is the current practice
593 for most railway infrastructure managers. Figures 11 and 12 compare lateral and vertical RMS
594 frequency weighted accelerations for extracts of the eight stretches with the same x and y scales
595 for all graphs. Moreover, Tables 6 and 7 list the mean RMS frequency weighted lateral acceleration
596 by sensor and ranked by magnitude. In these Tables, *M* stands for the mean signal calculated from
597 the sensors group.

598

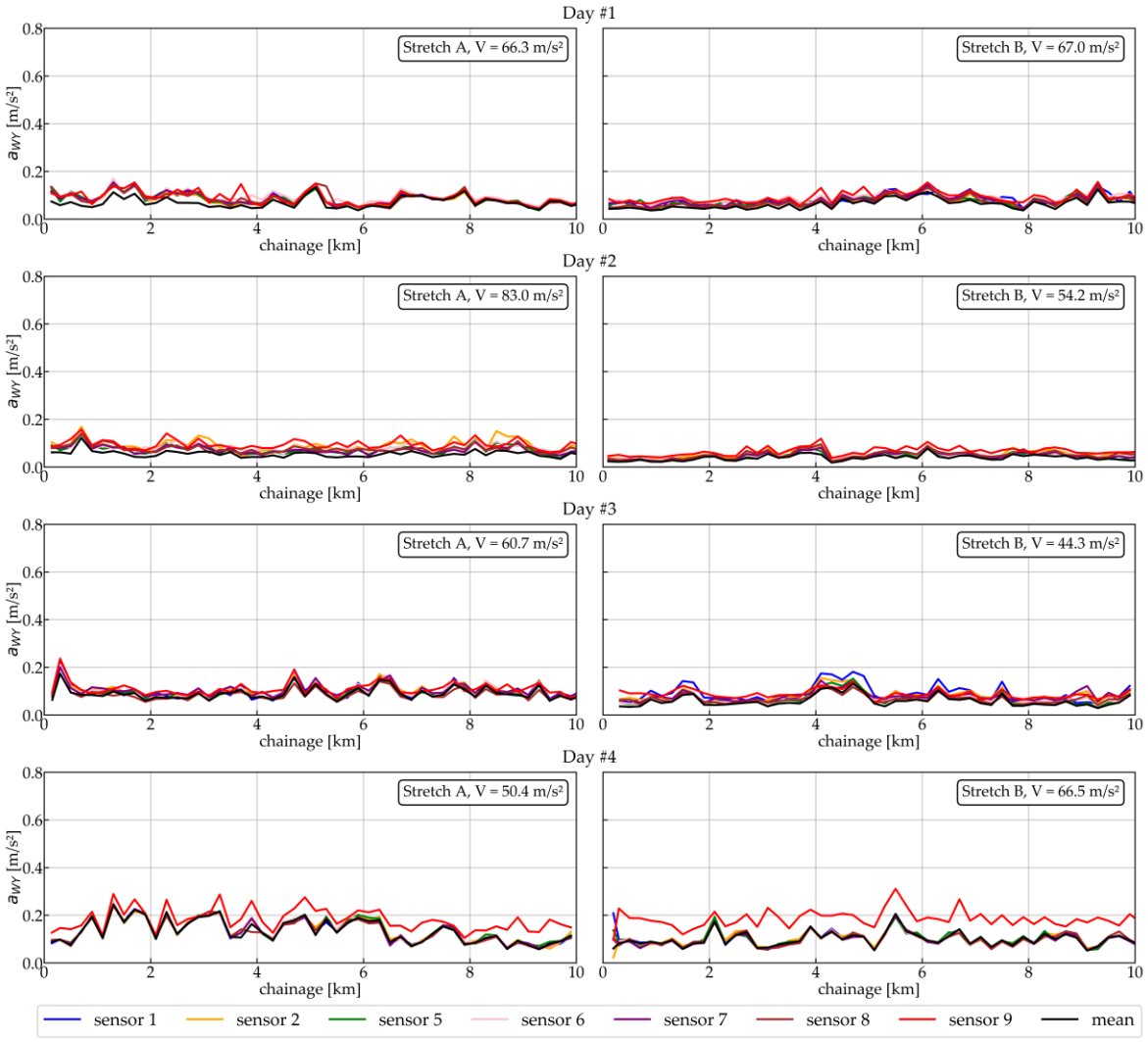

Figure 11. Root-mean-square frequency weighted lateral acceleration comparison, excerpts for the eight stretches

Table 6. Ranked mean RMS frequency weighted lateral acceleration by sensor

Day #1				Day #2				Day #3				Day #4			
A		B		A		B		A		B		A		B	
Sensor	Mean [m/s²]	Sensor	Mean [m/s²]	Sensor	Mean [m/s²]	Sensor	Mean [m/s²]	Sensor	Mean [m/s²]	Sensor	Mean [m/s²]	Sensor	Mean [m/s²]	Sensor	Mean [m/s²]
6	0.09	9	0.09	9	0.09	9	0.07	9	0.11	1	0.09	9	0.18	9	0.14
9	0.09	6	0.09	2	0.08	2	0.06	2	0.11	9	0.09	5	0.14	2	0.10
7	0.08	7	0.08	6	0.08	8	0.05	7	0.11	2	0.08	2	0.14	6	0.09
5	0.08	5	0.08	8	0.07	6	0.05	6	0.10	7	0.08	6	0.14	1	0.09
8	0.08	1	0.08	7	0.07	5	0.05	1	0.10	6	0.07	7	0.14	5	0.09
1	0.08	2	0.07	5	0.07	7	0.05	5	0.10	5	0.07	M	0.13	8	0.09
2	0.08	8	0.07	M	0.05	M	0.04	M	0.09	8	0.07	1	0.13	7	0.09
M	0.07	M	0.07	-	-	-	-	8	0.09	M	0.06	8	0.13	M	0.09

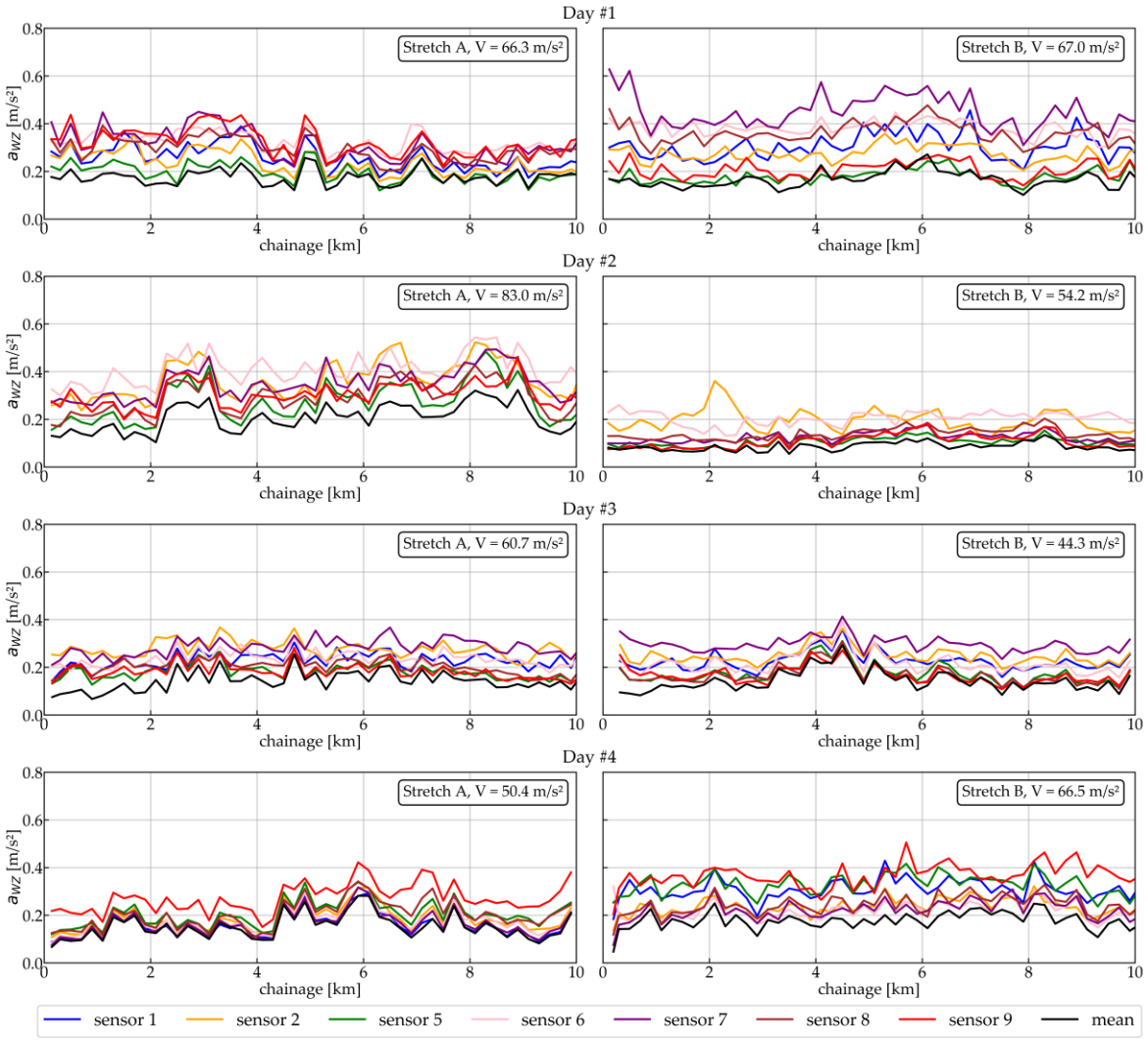

606

607 **Figure 12**. Root-mean-square frequency weighted vertical acceleration comparison, excerpts for
608 the eight stretches

609 **Table 7.** Ranked mean RMS frequency weighted vertical acceleration by sensor

Day #1				Day #2				Day #3				Day #4			
A		B		A		B		A		B		A		B	
Sensor	Mean [m/s²]	Sensor	Mean [m/s²]	Sensor	Mean [m/s²]	Sensor	Mean [m/s²]	Sensor	Mean [m/s²]	Sensor	Mean [m/s²]	Sensor	Mean [m/s²]	Sensor	Mean [m/s²]
6	0.33	7	0.41	6	0.41	6	0.22	7	0.28	7	0.30	9	0.27	9	0.34
9	0.33	6	0.37	7	0.35	2	0.21	2	0.27	2	0.25	5	0.20	5	0.31
7	0.31	8	0.34	2	0.35	8	0.15	6	0.23	1	0.23	8	0.20	1	0.29
8	0.29	1	0.28	9	0.29	7	0.14	1	0.22	6	0.22	2	0.19	8	0.23
1	0.25	2	0.26	8	0.27	9	0.13	8	0.20	5	0.17	6	0.17	2	0.23
2	0.24	9	0.20	5	0.25	5	0.11	9	0.18	8	0.17	7	0.16	6	0.22
5	0.19	5	0.18	M	0.19	M	0.10	5	0.18	9	0.17	1	0.16	7	0.22
M	0.17	M	0.17	-	-	-	-	M	0.14	M	0.14	M	0.15	M	0.17

610

611

Regarding arrangements in which sensors were distributed, it is not possible to identify a clear correlation between sensor position and a higher/smaller vibration magnitude since the magnitude of variation among the sensors is similar to those presented for the first day and thus may be mainly due to the sensor characteristics. For example, the sensor 5 yields for both stretches on the second day the smallest or the second smallest magnitude, expected behaviour for a sensor placed at the centre of the coach. However, its nearest neighbour does not present the same behaviour, contrary to the expected influence of sensor position on the obtained magnitude. For the third day, vertical acceleration, the sensors 7 and 2 have the greatest vibration for both stretches, but the magnitude of the difference could also be explained by sensor variation instead of possible suspension variation from a coach to another one. The same is said about the higher acceleration yielded by the sensor 9 on the fourth day, which should be investigated whether this is due to its position.

Table 8 presents the statistical summary of the correlation coefficients calculated for the RMS vertical and lateral frequency weighted accelerations for all selected stretches. In turn, Table 9 shows the ranking of the cross-correlation coefficients for each pair of RMS frequency weighted vertical accelerations also for all stretches. In this table, *pair* stands for the sensor pair with which the coefficient is associated. Moreover, Table 10 has the mean correlation coefficients by sensor to enable the identification of grating sensors. In complement, Figure 13 presents the same information as in Table 9 in boxplots to illustrate the sensor population dispersion and enable comparisons between days and between stretches. For brevity, the detailed correlation analysis considers only the vertical acceleration as a representative example.

This statistical analysis on correlation coefficients shows that the different sensor arrangements yielded similar collective behaviour, i.e., similar dispersions. It was expected that arrangements in which sensors were at approximately the same point or on the same transversal section would yield a greater agreement among sensors. Moreover, the coefficients' ranking and the boxplot do not reflect the position influence on measurements on the second day. Regarding this day, the high correlations between sensors even at positions with different vibration signatures (i.e., sensor 5 at the centre section of the coach and sensor 9 over the bogie) evidence the prevalence of sensor inherent variation on the results.

These remarks contribute to the conclusion that sensor-to-sensor variability (linked to sensor-to-sensor repeatability) influence is at least of the same magnitude of the variability driven by the position variation influence. The exception to be analysed during validation is the isolated behaviour of the sensor 9 on the fourth day.

Table 8. Statistical summary of the correlation coefficients

Day	Stretch	Mean r		Standard deviation r	
		Y	Z	Y	Z
Day #1	A	.90	.74	.06	.09
	B	.86	.66	.06	.12
Day #2	A	.78	.84	.08	.05
	B	.92	.75	.04	.18
Day #3	A	.90	.66	.06	.13
	B	.86	.86	.07	.05
Day #4	A	.94	.92	.06	.06
	B	.84	.75	.18	.17

647 **Table 9.** Ranking of the correlation coefficients for the RMS frequency weighted vertical
648 acceleration

Day #1				Day #2				Day #3				Day #4			
A		B		A		B		A		B		A		B	
Pair	r	Pair	r	Pair	r	Pair	r	Pair	r	Pair	r	Pair	r	Pair	r
5-9	.85	2-9	.85	5-8	.91	7-9	.95	5-8	.96	5-9	.89	2-7	.91	6-7	.98
7-8	.82	1-5	.85	8-9	.89	5-9	.94	6-8	.94	8-9	.85	7-8	.91	1-7	.98
2-8	.80	7-9	.84	2-8	.89	5-7	.94	5-6	.94	5-8	.83	6-7	.91	2-6	.97
1-8	.76	8-9	.81	5-7	.88	8-9	.94	2-5	.91	1-5	.77	2-6	.90	1-6	.97
1-7	.75	7-8	.81	2-5	.87	5-8	.93	2-8	.90	6-9	.71	6-8	.90	1-2	.97
1-2	.74	6-9	.80	5-9	.87	7-8	.93	1-6	.89	5-6	.71	2-8	.90	2-7	.97
2-9	.73	1-8	.80	7-8	.87	5-6	.74	8-9	.88	2-9	.68	1-2	.84	5-6	.96
8-9	.73	1-2	.79	2-9	.85	6-8	.73	2-6	.87	1-8	.68	5-8	.84	5-7	.96
6-8	.72	2-7	.79	5-6	.82	6-7	.70	1-5	.87	1-9	.67	2-5	.83	2-5	.96
2-7	.70	1-9	.77	2-7	.82	6-9	.69	5-9	.86	2-5	.66	5-7	.83	5-8	.95
6-7	.69	2-8	.76	7-9	.81	2-7	.63	1-8	.86	1-6	.66	5-6	.82	1-5	.94
2-6	.68	1-7	.73	6-8	.80	2-8	.61	7-8	.86	6-7	.65	1-7	.80	7-8	.92
2-5	.65	6-7	.72	6-7	.76	2-5	.59	1-2	.85	5-7	.65	1-8	.80	8-9	.92
1-9	.64	2-6	.72	2-6	.75	2-9	.58	2-9	.84	1-7	.64	1-5	.79	2-8	.91
5-8	.61	5-8	.72	6-9	.75	2-6	.38	6-9	.84	7-9	.62	1-6	.77	6-8	.91
1-5	.59	6-8	.70	-	-	-	-	5-7	.83	6-8	.62	8-9	.52	1-8	.88
1-6	.59	2-5	.69	-	-	-	-	7-9	.83	2-8	.62	5-9	.50	5-9	.87
6-9	.57	5-7	.63	-	-	-	-	6-7	.83	7-8	.58	7-9	.49	7-9	.84
7-9	.53	5-9	.61	-	-	-	-	1-9	.78	2-6	.52	2-9	.49	6-9	.83
5-6	.42	1-6	.61	-	-	-	-	2-7	.78	1-2	.52	1-9	.48	2-9	.81
5-7	.37	5-6	.48	-	-	-	-	1-7	.74	2-7	.31	6-9	.47	1-9	.78

649

650 **Table 10.** Statistical summary of the correlation coefficients by sensor for the vertical acceleration

Day	Stretch	Mean r by sensor						
		1	2	5	6	7	8	9
Day #1	A	.76	.77	.67	.67	.75	.77	.78
	B	.68	.72	.58	.61	.64	.74	.68
Day #2	A	-	.84	.87	.78	.83	.87	.83
	B	-	.56	.83	.65	.83	.83	.82
Day #3	A	.66	.55	.75	.65	.58	.70	.74
	B	.83	.86	.90	.89	.81	.90	.84
Day #4	A	.92	.93	.94	.94	.94	.92	.84
	B	.75	.81	.77	.79	.81	.81	.49

651

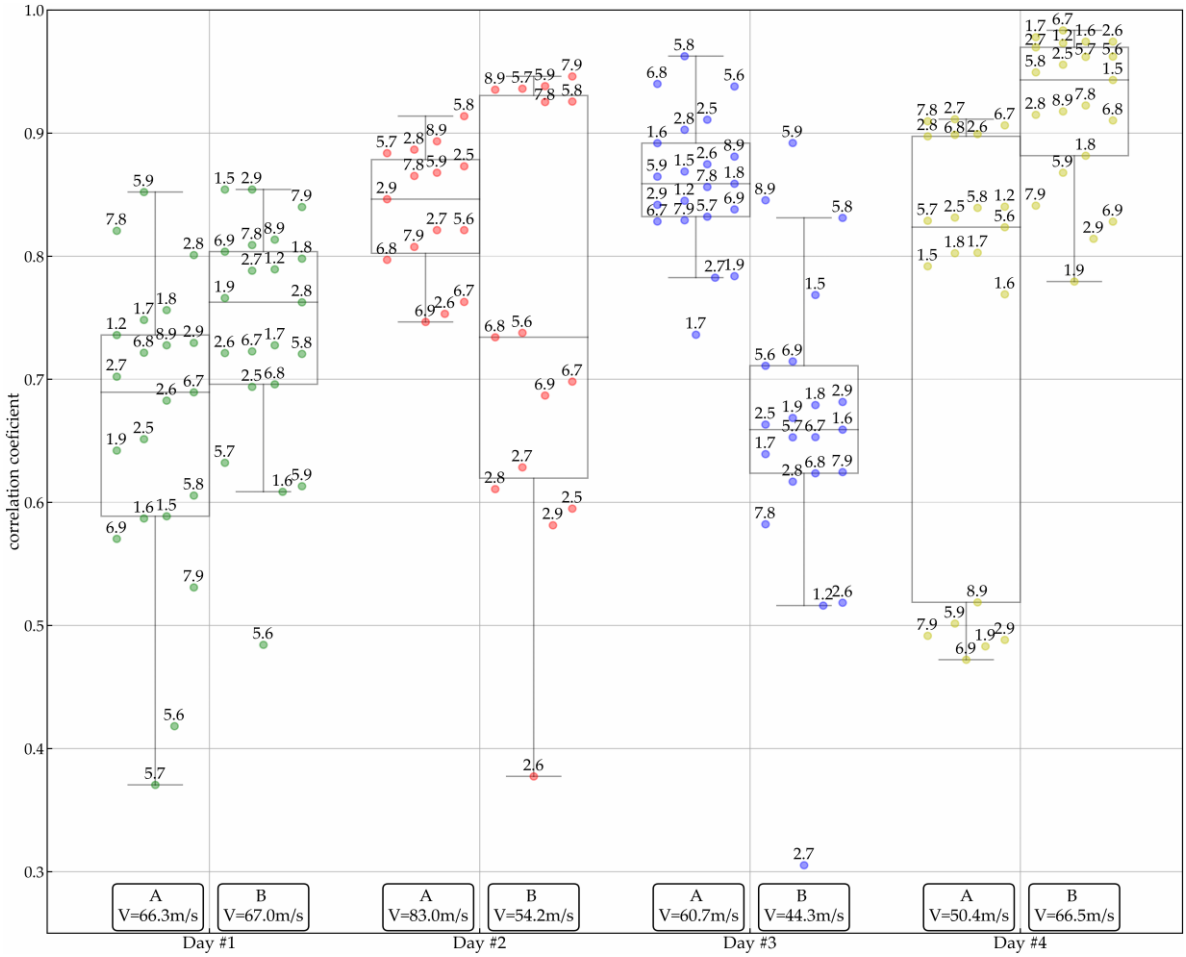

Figure 13. Boxplot of the correlation coefficients for the RMS frequency weighted vertical acceleration

4.4 Comfort results validation

Ideally, validation should be performed for all sensor configurations, but only data for the fourth day, stretch B, was made available. To provide an overview of the track quality on this stretch, Figure 14 depicts the longitudinal level and alignment data for ranges D1 and D2 gathered by the *Treno Diamante*. The figure also shows the maximum alert limits for speeds between 230 and 300 km/h as stated by the EN 13848-5 [92]. These limit values are merely indicative and reflect the common European practice but may change according to the infrastructure managers' maintenance policy.

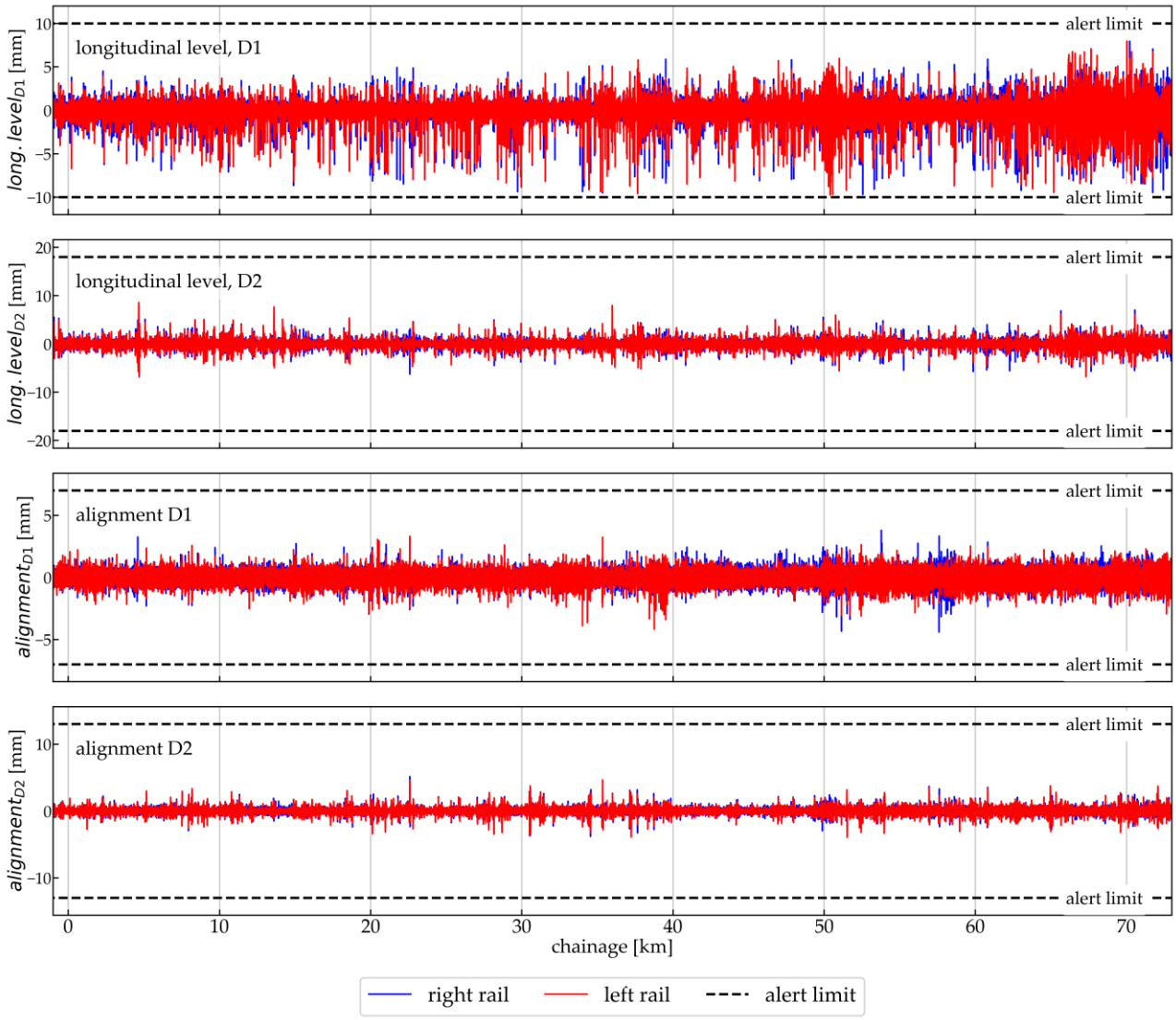

Figure 14. Track longitudinal level and alignment (ranges D1 and D2) for the fourth day, stretch B.

For this validation, the comparison with reference data considered calculating the correlation coefficients between each sensor response (including the mean signal and the mean RMS) and the track parameters (standard deviation). Validation results are presented in Tables 11 and 12 for, respectively, the lateral and vertical directions. For brevity, only parameters that present coefficients greater than 0.4 for the mean signal are presented. Besides the mean signal for all signals, it was also analysed the mean signal excluding the sensor 9 since its performance was discrepant. From validation tables, sensor 9 presents a much smaller correlation with track parameters, and it can be concluded that its discrepant behaviour on stretch B is probably due to sensor malfunctioning rather than to a more irregular track on the right side. Another relevant aspect is that, for the vertical direction, the mean signal without the sensor 9 yields a result almost as good as the best sensor in terms of correlation with track features, which indicates the suitability of measuring strategies based on the mean signal.

As an expected validation result, the lateral and vertical accelerations are significantly correlated with, respectively, alignment and longitudinal level. In addition, a higher correlation is observed with left side parameters than with their homologues on the right side, a predictable result given their installation on this side on the train cabin (left side considering the normal train orientation, right side considering train moving backwards on 4th day). It can also be concluded that longitudinal short and medium wavelengths (10-m chord, D1 and D2) contribute most to frequency

683 weights results, another expected result given the high-pass filter used in ISO-2613 analysis with a
684 corner frequency of about 0.4 Hz. Thus, features with wavelengths over about 160 m are not
685 considered.

686 **Table 11.** Correlation between sensors responses and track parameters, lateral acceleration

Parameter	Sensor 1	Sensor 2	Sensor 5	Sensor 6	Sensor 7	Sensor 8	Sensor 9	Mean signal (1-9)	Mean signal (1-8)	Mean RMS (1-8)
Alignment, left, D2	.60	.60	.57	.60	.59	.58	.28	.51	.50	.60
Alignment, right, D2	.59	.59	.57	.60	.59	.59	.25	.50	.49	.60
Alignment, total, D1	.48	.52	.48	.51	.50	.49	.22	.43	.42	.51
Alignment, left, D1	.43	.48	.45	.46	.47	.44	.32	.44	.42	.46
Superelevation deviation	.39	.44	.42	.42	.41	.42	.05	.38	.40	.42

687 **Table 12.** Correlation between sensors responses and track parameters, vertical acceleration

Parameter	Sensor 1	Sensor 2	Sensor 5	Sensor 6	Sensor 7	Sensor 8	Sensor 9	Mean signal (1-9)	Mean signal (1-8)	Mean RMS (1-8)
Longitudinal level, total, D1	.69	.84	.70	.86	.85	.82	.30	.84	.85	.85
Longitudinal level, left, D1	.65	.80	.65	.82	.82	.80	.36	.83	.82	.81
Longitudinal level, left, 10-m	.64	.79	.65	.81	.82	.79	.36	.82	.82	.80
Longitudinal level, right, D1	.66	.75	.64	.76	.78	.74	.21	.75	.76	.77
Longitudinal level, right, 10m	.65	.75	.64	.76	.77	.74	.22	.75	.76	.77
Cross level	.59	.66	.56	.67	.66	.63	.33	.60	.61	.67
Superelevation deviation	.58	.64	.55	.63	.66	.62	.35	.6	.61	.66
Cross level deviation, 10-m	.58	.65	.55	.63	.65	.62	.33	.59	.60	.65
Longitudinal level, left, D2	.37	.49	.43	.53	.51	.51	.27	.54	.52	.51
Longitudinal level, right, D2	.39	.46	.43	.48	.48	.48	.19	.50	.49	.49
Twist, 3-m	.41	.50	.40	.48	.50	.46	.23	.45	.46	.49

688 Moreover, Figures 15 and 16 depict the mean lateral and vertical signals (sensors 1 to 8) and
689 compare them with the most correlated track parameters, allowing for visual confirmation of the
690 concordance between results and reference data. For clarity, this comparison was separated into
691 two graphs for each axis.

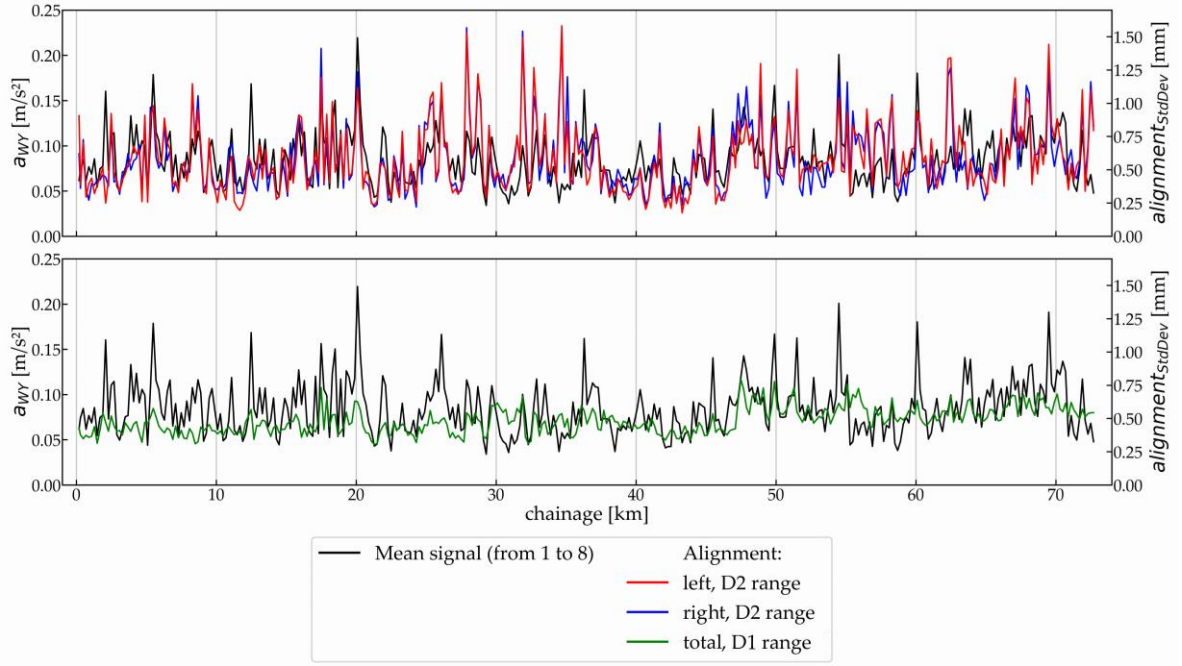

692

693 **Figure 15.** Root-mean-square frequency weighted lateral acceleration (mean signal) versus
694 alignment (standard deviation, range D2 on top subplot and total range D1 on bottom subplot)

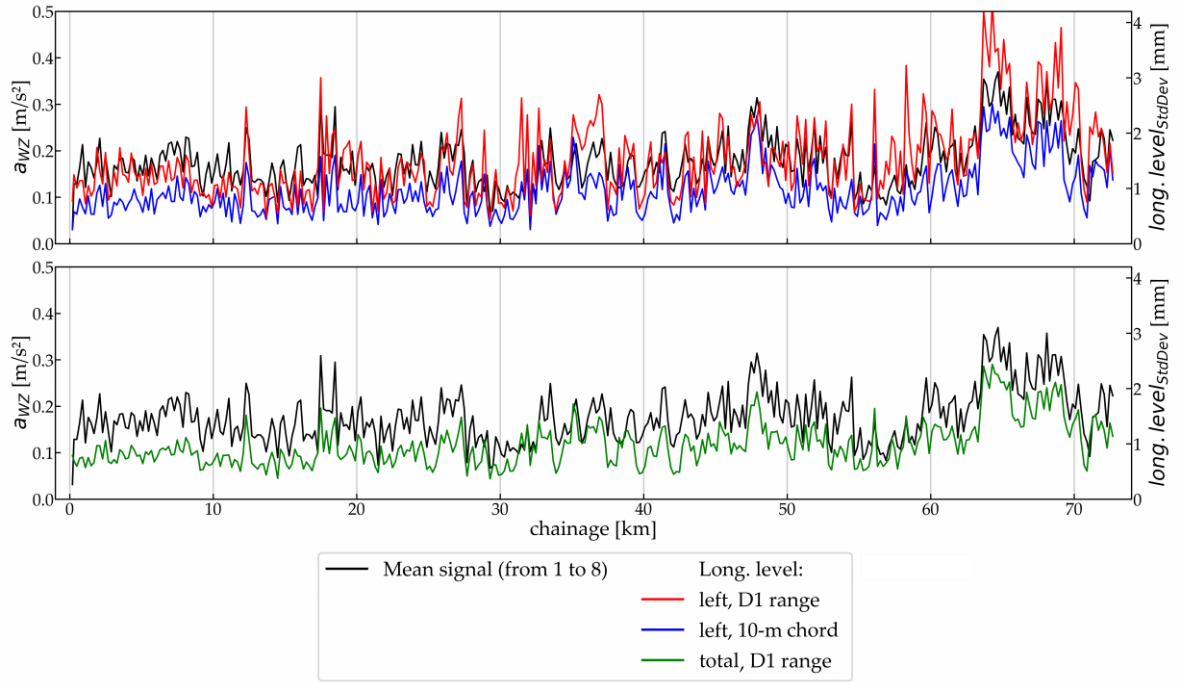

695

696 **Figure 16.** Root-mean-square frequency weighted vertical acceleration (mean signal) versus
697 longitudinal level (standard deviation, range D1 and 10-m on top subplot, total 10-m on bottom
698 subplot)

699 Regarding lateral acceleration, the worse performance of the mean signal may result from the
700 discrepant behaviour of some sensors during subintervals of the considered stretch (intervals with
701 more significant discordance among sensors from about 30-km chainage). Therefore, the same
702 comparison with reference data was performed only for the first 130 sections for lateral
703 acceleration, in which sensors are the most concordant. The results presented in Table 13 show
704 similar individual behaviour for the majority regarding the most correlated parameters but a
705 considerably better performance of the mean signal. By adopting this subset, the mean signal

behaves like for the vertical direction and yields results that virtually are as good as those of the best sensors. Thus, collective result quality depends on a previous analysis for sensor group concordance. Furthermore, the smaller coefficient correlation for lateral is expected given the relative motion between wheelset and the consequent smaller correlation between lateral displacements and lateral irregularities.

Table 13. Correlation between sensors responses and track parameters, lateral acceleration for the first 130 sections

Parameters	Sensor 1	Sensor 2	Sensor 5	Sensor 6	Sensor 7	Sensor 8	Sensor 9	Mean signal (1-9)	Mean signal (1-8)	Mean RMS (1-8)
Alignment, right, D2	.58	.59	.58	.59	.60	.60	.34	.59	.60	.60
Alignment, total, D1	.55	.55	.57	.57	.60	.59	.34	.58	.58	.58
Alignment, left, D2	.60	.57	.57	.58	.59	.59	.30	.57	.58	.60
Alignment, right, D1	.54	.51	.54	.54	.57	.55	.34	.54	.55	.56
Alignment, right, 10-m	.50	.47	.51	.50	.54	.52	.35	.50	.51	.52
Superelevation deviation	.32	.49	.45	.44	.43	.42	.29	.46	.46	.43
Alignment, left, D1	.36	.45	.43	.43	.44	.44	.33	.47	.46	.44
Longitudinal level, right, D2	.40	.41	.51	.40	.44	.38	.34	.43	.43	.43
Longitudinal level, right, D3	.36	.42	.46	.39	.41	.38	.30	.42	.41	.41
Longitudinal level, total, D1	.39	.40	.43	.41	.42	.40	.30	.41	.41	.42
Longitudinal level, left, D3	.37	.40	.44	.39	.40	.38	.31	.40	.40	.40
Cross level	.42	.37	.41	.41	.41	.38	.25	.38	.40	.41

Lastly, it is noteworthy that some of the significant correlations obtained and presented in the tables above may be due not to direct causation but due to indirect relationship given by the intrinsic correlation between track parameters since irregularities can develop from common local-dependent causes such as ballast and subgrade conditions or they are geometrically dependent. As expected, left and right measurements of longitudinal level are highly correlated (greater than 0.87 for the analysed stretch). As another example, the alignment in range D1 has correlations varying from 0.18 with longitudinal level in range D2 to 0.58 with gauge. In addition, the cross level and its derived parameters (cross-level deviation within a 10-m window and the superelevation deviation) are obviously highly correlated ($r > 0.92$). Nevertheless, controlling for the spurious associations is not in the present scope since the aim is merely to verify whether comfort results are adherent to track quality in general terms.

5 Conclusions

The tests carried out aboard a track recording vehicle of the Italian railway high-speed network assessed the feasibility of a track monitoring system based on very low-cost sensors. The coherent behaviour of the sensor collectivity in different arrangements, which aimed to test the influence of sensor position on the quality of the measurements, evidenced the limitations and potentialities of the proposed collective use of sensors. Since the expected influence of sensor position on measurements was not identified, it can be concluded that the sensor-to-sensor variability of the very low-quality sensors does not allow for this nuanced vibration differentiation. On the other hand, the good agreement among the sensors shows that the proposed device can yield repeatable outputs and that the collective approach enables the identification of discrepant measurements.

The validation of root-mean-square frequency weighted accelerations demonstrated a strong correlation between vertical measurements and longitudinal level (range D1, total, $r = 0.86$ for the best signal), as well as a moderate correlation between lateral measurements and alignment (range D2, right, $r = 0.60$ for the best signal). These results are coherent with expected train behaviour under track solicitation. Regarding the collective approach and the mean vibrations response (excluded the discrepant signal), the resulting correlation was almost as good as that

yielded by the best matching sensor, which indicates the suitability of using the fused signal of a sensor group as a robust comfort or track quality index. Hence, since the mean signals preserved the group relationship with track features, it can be concluded that the smaller RMS estimates from the sensor combination may be mainly due to noise reduction than to information loss. However, unexpected behaviour on validation of lateral vibration demonstrated the need for outlier detection algorithms to curb the influence on calculated mean not only of the discrepant sensors but also of the momentarily discrepant signal, probably through windowed cross-correlation analysis and elimination of discrepant measurement by each section.

Further work will encompass analyses of the relationship between other aspects of the measurement context (train speed and track quality level) and the quality of measurements (variation within the sensor population and correlation of result with reference data). The methods presented in this work proved to be suitable for such analyses and will be replicated for the entire trips. Complementary, a windowed algorithm for discrepant signal identification should be studied considering an entire trip to define the most appropriate thresholds for sensor exclusion. For these tasks, reference data should be made available for all the high-speed network for the appropriate continuation of the research.

Authors' Contributions: Rafael Henrique de Oliveira: Conceptualisation, Data curation, Formal analysis, Investigation, Methodology, Software, Validation, Visualisation, Writing - original draft. **Giuseppe Loprencipe:** Methodology, Funding acquisition, Project administration, Resources, Supervision, Writing - review & editing. **Flávio Guilherme Vaz de Almeida Filho:** Methodology, Funding acquisition, Project administration, Resources, Supervision, Writing - review & editing. **Rodrigo de Sousa Pissardini**: Conceptualisation, Methodology, Writing - review & editing.

Funding: This research was funded in part by the *Coordenação de Aperfeiçoamento de Pessoal de Nível Superior* (CAPES), Brazil, Finance Code 001.

Acknowledgements: The Authors thank the Mobile Diagnostics Department of the Italian Railway Infrastructure Manager (*Rete Ferroviaria Italiana*), in particular Eng. Marco Gallini, Eng. Gennaro Alteriso, and Eng. Giorgio Perrotta for the immeasurable collaboration during the tests with the *Diamante* train and the data sharing.

Data Availability Statement: Not applicable.

Conflicts of Interest: The authors declare no conflict of interest.

References

1. Pita, A.L. *Infraestructuras Ferroviarias*; Edicions de la Universitat Politècnica de Catalunya: Barcelona, 2006;
2. Weston, P.; Roberts, C.; Yeo, G.; Stewart, E. Perspectives on railway track geometry condition monitoring from in-service railway vehicles. *Veh. Syst. Dyn.* 2015, *53*, 1063–1091, doi:10.1080/00423114.2015.1034730.
3. Nielsen, J.; Berggren, E.G.; Lölgen, T.; Müller, R.; Stallaert, B.; Pesqueux, L. Overview of Methods for Measurement of Track Irregularities for Ground-Borne Vibration - Deliverable D2.5. *Chalmers Univ. Technol. Trafikverkt, DB, SBB, D2S Int. Alstom* 2013, 1–49.
4. Stow, J.; Andersson, E. Field testing and instrumentation of railway vehicles. In *Handbook of Railway Vehicle Dynamics*; Iwnicki, S., Ed.; Taylor & Francis Group: London, UK, 2006.
5. Matisa Véhicules d'auscultation sur la voie du succès - L'optimisation de la gestion des réseaux. 2017.
6. Société Nationale des Chemins de Fer Français The IRIS 320 High Speed Measurement Train Set 2008, 1–11.
7. Zucchi, E. La qualità del binario nelle linee AV/AC : studio dei dati rilevati dai treni diagnostici di RFI e analisi degli interventi manutentivi in previsione dell'aumento di velocità a 360 km/h, Università di Bologna, 2013.
8. Network Rail *Train Infrastructure Interface Specification (TIIS) - IEP-TEHC-REQ-36*;

Network Rail, Ed.; Issue 03.; Network Rail: London, UK, 2007;
9. Bocciolone, M.; Caprioli, A.; Cigada, A.; Collina, A. A measurement system for quick rail inspection and effective track maintenance strategy. *Mech. Syst. Signal Process.* 2007, *21*, 1242–1254, doi:10.1016/j.ymssp.2006.02.007.
10. Bongini, E.; Grassie, S.; Saxon, M. 'Noise Mapping'of a Railway Network: Validation and Use of a System Based on Measurement of Axlebox Vibration. *Noise Vib. Mitig. Rail …* 2012, 1–8.
11. Du, Y.; Sun, B.; Li, F.; Ma, H.; Zhang, W.; Huang, W. Detection of rail corrugation based on fiber laser accelerometers. *Meas. Sci. Technol.* 2013, *24*, 094014, doi:10.1088/0957-0233/24/9/094014.
12. Real, J.I.; Montalbán, L.; Real, T.; Puig, V. Development of a system to obtain vertical track geometry measuring axle-box accelerations from inservice trains. *J. Vibroengineering* 2012, *14*, 813–826.
13. Li, Z.; Molodova, M.; Nunez, A.; Dollevoet, R. Improvements in Axle Box Acceleration Measurements for the Detection of Light Squats in Railway Infrastructure. *IEEE Trans. Ind. Electron.* 2015, *62*, 4385–4397, doi:10.1109/TIE.2015.2389761.
14. Wang, P.; Cui, D.; An, B.; Chen, R.; Xu, J. Observation and Simulation of Axle Box Acceleration in the Presence of Rail Weld in High-Speed Railway. *Appl. Sci.* 2017, *7*, 1259, doi:10.3390/app7121259.
15. Weston, P.F.; Ling, C.S.; Roberts, C.; Goodman, C.J.; Li, P.; Goodall, R.M. Monitoring lateral track irregularity from in-service railway vehicles. *Proc. Inst. Mech. Eng. Part F J. Rail Rapid Transit* 2007, *221*, 89–100, doi:10.1243/0954409JRRT65.
16. Iontchev, E.; Kenov, R.; Miletiev, R. Inertial measurement system for evaluation of the bogie-railway system dynamics. *Proc. Int. Spring Semin. Electron. Technol.* 2013, 345–348, doi:10.1109/ISSE.2013.6648270.
17. Abuhamdia, T.; Taheri, S.; Meddah, A.; Davis, D. Rail Defect Detection Using Data From Tri-Axial Accelerometers. 2014, V001T06A001, doi:10.1115/jrc2014-3703.
18. Quirke, P.; Cantero, D.; Obrien, E.J.; Bowe, C. Drive-by detection of railway track stiffness variation using in-service vehicles. *Proc. Inst. Mech. Eng. Part F J. Rail Rapid Transit* 2017, *231*, 498–514, doi:10.1177/0954409716634752.
19. Zoccali, P.; Loprencipe, G.; Lupascu, R.C. Acceleration measurements inside vehicles: Passengers' comfort mapping on railways. *Meas. J. Int. Meas. Confed.* 2018, *129*, 489–498, doi:10.1016/j.measurement.2018.07.079.
20. Paixão, A.; Fortunato, E.; Calçada, R. Smartphone's Sensing Capabilities for On-Board Railway Track Monitoring: Structural Performance and Geometrical Degradation Assessment. *Adv. Civ. Eng.* 2019, *2019*, doi:10.1155/2019/1729153.
21. Seraj, F.; Meratnia, N.; Havinga, P.J.M. RoVi: Continuous transport infrastructure monitoring framework for preventive maintenance. *2017 IEEE Int. Conf. Pervasive Comput. Commun. PerCom 2017* 2017, 217–226, doi:10.1109/PERCOM.2017.7917868.
22. Lederman, G.; Chen, S.; Garrett, J.; Kovacevic, J.; Noh, H.Y.; Bielak, J. Track-monitoring from the dynamic response of an operational train. *Mech. Syst. Signal Process.* 2017, *87*, 1–16, doi:10.1016/j.ymssp.2016.06.041.
23. Do, N.T.; Abdulrazagh, P.H.; Gül, M.; Hendry, M.T.; Roghani, A.; Toma, E. Evaluating passenger railway ride quality over long distances using smartphones. *2020 Jt. Rail Conf. JRC 2020* 2020, doi:10.1115/JRC2020-8093.
24. NeTIRail-INFRA Deliverable D4.6Low cost smartphone based track and ride quality monitoring technology. 2017.
25. Weston, P.; Roberts, C.; Yeo, G.; Stewart, E. Perspectives on railway track geometry condition monitoring from in-service railway vehicles. *Veh. Syst. Dyn.* 2015, *53*, 1063–1091, doi:10.1080/00423114.2015.1034730.
26. Dow, A. *The Railway: British Track Since 1804*; Pen \& Sword Books Limited, 2014; ISBN 9781473822573.
27. International Organization for Standardization ISO 10056 - Mechanical vibration - Measurement and analysis of whole-body vibration to which passengers and crew are exposed in railway vehicles. 2003, *2003*, 13.
28. Hungria, L.H. *Segurança operacional de trens de carga*; All Print Editora: São Paulo, 2017;

29. Grassie, S.L. Measurement of railhead longitudinal profiles: A comparison of different techniques. *Wear* 1996, *191*, 245–251, doi:10.1016/0043-1648(95)06732-9.
30. Wei, Z.; Boogaard, A.; Nunez, A.; Li, Z.; Dollevoet, R. An integrated approach for characterizing the dynamic behavior of the wheel-rail interaction at crossings. *IEEE Trans. Instrum. Meas.* 2018, *67*, 2332–2344, doi:10.1109/TIM.2018.2816800.
31. Zhu, X.Q.; Law, S.S.; Huang, L. Identification of Railway Ballasted Track Systems from Dynamic Responses of In-Service Trains. *J. Aerosp. Eng.* 2018, *31*, 04018060, doi:10.1061/(asce)as.1943-5525.0000898.
32. Wickens, A.H. A History of Railway Vehicle Dynamics. In *Handbook of Railway Vehicle Dynamics*; Iwnicki, S., Ed.; Taylor & Francis Group: London, UK, 2006.
33. Kraft, S.; Causse, J.; Coudert, F. Vehicle response-based track geometry assessment using multi-body simulation. *Veh. Syst. Dyn.* 2018, *56*, 190–220, doi:10.1080/00423114.2017.1359418.
34. Li, C.; Luo, S.; Cole, C.; Spiryagin, M. An overview: modern techniques for railway vehicle on-board health monitoring systems. *Veh. Syst. Dyn.* 2017, *55*, 1045–1070, doi:10.1080/00423114.2017.1296963.
35. Salvador, P.; Naranjo, V.; Insa, R.; Teixeira, P. Axlebox accelerations: Their acquisition and time-frequency characterisation for railway track monitoring purposes. *Meas. J. Int. Meas. Confed.* 2016, *82*, 301–312, doi:10.1016/j.measurement.2016.01.012.
36. Vinkó, Á.; Bocz, P. Experimental investigation on condition monitoring opportunities of tramway tracks. *Period. Polytech. Civ. Eng.* 2018, *62*, 180–190, doi:10.3311/PPci.10541.
37. Haigermoser, A.; Luber, B.; Rauh, J.; Gräfe, G. Road and track irregularities: Measurement, assessment and simulation. *Veh. Syst. Dyn.* 2015, *53*, 878–957, doi:10.1080/00423114.2015.1037312.
38. Thompson, D.; Jones, C. Noise and Vibration from Railway Vehicles. In *Handbook of Railway Vehicle Dynamics*; Iwnicki, S., Ed.; Taylor & Francis Group, 2006.
39. Iwnick, S. Manchester Benchmarks for Rail Vehicle Simulation Manchester Benchmarks for Rail Vehicle Simulation. 2007, 37–41.
40. Polach, O.; Berg, M.; Iwnicki, S. Simulation. In *Handbook of Railway Vehicle Dynamics*; Iwnicki, S., Ed.; Taylor & Francis Group, 2006; pp. 359–422.
41. Comité Européen de Normalisation EN 13848-5 - 2017 - Railway applications - Track - Track geometry quality - Part 5: Geometric quality levels - Plain line, switches and crossings 2017.
42. Garg, V.K.; Dukkipati, R. V. *Dynamics of railway vehicle systems*; Academic Press, 1984;
43. Cole, C. Longitudinal Train Dynamics. In *Handbook of Railway Vehicle Dynamics*; Iwnicki, S., Ed.; Taylor & Francis Group, 2006.
44. Hoberock, L.L. A survey of longitudinal acceleration comfort studies in ground transportation vehicles. *J. Dyn. Syst. Meas. Control. Trans. ASME* 1977, *99*, 76–84, doi:10.1115/1.3427093.
45. Comité Européen de Normalisation EN 13848-6 - 2014 - Railway applications - Track - Track geometry quality - Part 6 - Characterisation of track geometry quality 2014, *44*.
46. Weston, P.F.; Ling, C.S.; Goodman, C.J.; Roberts, C.; Li, P.; Goodall, R.M. Monitoring lateral track irregularity from in-service railway vehicles. *Proc. Inst. Mech. Eng. Part F J. Rail Rapid Transit* 2007, *221*, 89–100, doi:10.1243/0954409JRRT64.
47. Alfi, S.; De Rosa, A.; Bruni, S. Estimation of lateral track irregularities from on-board measurement: Effect of wheel-rail contact model. *IET Conf. Publ.* 2016, *2016*, 1–7, doi:10.1049/cp.2016.1205.
48. Tanifuji, K. A vertical vibration analysis of coupled bogie cars in a train for evaluation of riding comfort. *Veh. Syst. Dyn.* 1988, *17*, 481–492, doi:10.1080/00423118808969289.
49. Kang, B.B. Influence of train length on the lateral vibration of a high-speed train equipped with articulated bogies. *J. Mech. Sci. Technol.* 2014, *28*, 3517–3527, doi:10.1007/s12206-014-0812-0.
50. Ingle, V.K.; Proakis, J.G. *Digital Signal Processing using MATLAB*; Brooks-Cole: Pacific Grove, 2000;
51. Manolakis, D.G.; Ingle, V.K.; Kogon, S.M. *Statistical and Adaptive Signal Processing: Spectral Estimation, Signal Modeling, Adaptive Filtering, and Array Processing*; Artech

House signal processing library; Artech House, 2005; ISBN 9781580536103.
52. Bhardwaj, B.; Bridgelall, R.; Lu, P.; Dhingra, N. Signal Feature Extraction and Combination to Enhance the Detection and Localization of Railroad Track Irregularities. *IEEE Sens. J.* 2020, *21*, 6555–6563, doi:10.1109/JSEN.2020.3041652.
53. Real, J.; Salvador, P.; Montalbán, L.; Bueno, M. Determination of rail vertical profile through inertial methods. *Proc. Inst. Mech. Eng. Part F J. Rail Rapid Transit* 2011, *225*, 14–23, doi:10.1243/09544097JRRT353.
54. OBrien, E.J.; Quirke, P.; Bowe, C.; Cantero, D. Determination of railway track longitudinal profile using measured inertial response of an in-service railway vehicle. *Struct. Heal. Monit.* 2018, *17*, 1425–1440, doi:10.1177/1475921717744479.
55. Odashima, M.; Azami, S.; Naganuma, Y.; Mori, H.; Tsunashima, H. Track geometry estimation of a conventional railway from car-body acceleration measurement. *Mech. Eng. J.* 2017, *4*, 16-00498-16–00498, doi:10.1299/mej.16-00498.
56. Molodova, M.; Li, Z.; Núñez, A.; Dollevoe, R. Automatic Detection of Squats in Railway Infrastructure. *IEEE Trans. Intell. Transp. Syst.* 2014, *18*, 1980–1990.
57. Vinkó, Á.; Bocz, P. Experimental investigation on condition monitoring opportunities of tramway tracks. *Period. Polytech. Civ. Eng.* 2018, *62*, 180–190, doi:10.3311/PPci.10541.
58. Barbosa, R.S. Evaluation of Railway Track Safety with a New Method for Track Quality Identification. *J. Transp. Eng.* 2016, *142*, 04016053, doi:10.1061/(asce)te.1943-5436.0000855.
59. Hong, K.C.; Hussin, F.A.; Saman, A.B.S. Automated train track misalignment detection system based on inertia measurement unit. *2014 IEEE Student Conf. Res. Dev. SCOReD 2014* 2014, 1–5, doi:10.1109/SCORED.2014.7072991.
60. Azzoug, A.; Kaewunruen, S. Ridecomfort: A development of crowdsourcing smartphones in measuring train ride quality. *Front. Built Environ.* 2017, *3*, 1–12, doi:10.3389/fbuil.2017.00003.
61. NeTIRail-INFRA Deliverable D4.11Validated monitoring equipment produced by testing of instrumentation in the real environment. 2018.
62. Authors [Title omitted for blind review]. 2021.
63. Invensense MPU-9250 Product Specification Revision 1.1 2019.
64. Bosch BMP280 Digital Pressure Sensor Bosch Sensortec Datasheet 1.14 2015, 49.
65. U-blox NEO-6 u-blox 6 GPS Modules. *Www.U-Blox.Com* 2017, 25.
66. Richards Tech RTIMULib2 - a versatile C++ and Python 9-dof, 10-dof and 11-dof IMU library Available online: https://github.com/RTIMULib/RTIMULib2.
67. Braam, M. Python3 GPSD client - a library for polling gpsd in Python3 Available online: https://github.com/MartijnBraam/gpsd-py3 (accessed on Dec 10, 2020).
68. International Organization for Standardization ISO 2631-1 - Mechanical vibration and shock - Evaluation of human exposure to whole-body vibration - Part 1: General requirements 1997, 31.
69. MERMEC Ride Quality Available online: http://www.mermecgroup.com/inspect/track-measurement/1019/ride-quality.php (accessed on Jul 20, 2020).
70. Moretti, M. Sul Diamante, il treno diagnostico che ora interessa ai giapponesi. *Sole 24 Ore* 2017.
71. Dickey, D.A. Stationarity Issues in Time Series Models. *SAS Glob. Forum* 2005, 1–17.
72. Titterton, D.H.; Weston, J.L. Strapdown Inertial Navigation Technology - 2nd Edition. 2004, 558, doi:10.1049/PBRA017E.
73. Heirich, O.; Lehner, A.; Robertson, P.; Strang, T. Measurement and analysis of train motion and railway track characteristics with inertial sensors. *IEEE Conf. Intell. Transp. Syst. Proceedings, ITSC* 2011, 1995–2000, doi:10.1109/ITSC.2011.6082908.
74. Mutter, H.; Simmonds, K..; Arnold, G..; Carter, B..; Irani, F.; Elkins, J.; Swearingen, B.; Dicrhe, R. *Metropolitan Atlanta Rapid Transit Authority - Transit vehicle engineering tests*; Pueblo, CO, 1981;
75. Euston, M.; Coote, P.; Mahony, R.; Kim, J.; Hamel, T. A complementary filter for attitude estimation of a fixed-wing UAV. *2008 IEEE/RSJ Int. Conf. Intell. Robot. Syst. IROS* 2008, 340–345, doi:10.1109/IROS.2008.4650766.
76. Vectornav IMU Specifications Available online: https://www.vectornav.com/resources/imu-

specifications (accessed on Apr 25, 2021).
77. Kohn, A.F. Autocorrelation and Cross-Correlation Methods. In *Wiley Encyclopedia of Biomedical Engineering*; Akay, M., Ed.; John Wiley & Sons Inc.: Hoboken, 2006; Vol. 1 ISBN 0-471-24967-X.
78. Guerrier, S. Integration of Skew-Redundant MEMS-IMU with GPS for Improved Navigation Performance, École Polytechnique Fédérale de Lausanne, 2008.
79. Fichera, G.; Scionti, M.; Garescì, F. Experimental correlation between the road roughness and the comfort perceived in bus cabins. *SAE Tech. Pap.* 2007, doi:10.4271/2007-01-0352.
80. Kırbaş, U.; Karaşahin, M. Investigation of ride comfort limits on urban asphalt concrete pavements. *Int. J. Pavement Eng.* 2018, *19*, 949–955, doi:10.1080/10298436.2016.1224413.
81. Ahlin, K.; Granlund, N.O.J. Relating Road Roughness and Vehicle Speeds to Human Whole Body Vibration and Exposure Limits. *Int. J. Pavement Eng.* 2002, *3*, 207–216, doi:10.1080/10298430210001701.
82. Loprencipe, G.; Zoccali, P. Ride quality due to road surface irregularities: Comparison of different methods applied on a set of real road profiles. *Coatings* 2017, *7*, doi:10.3390/coatings7050059.
83. Zhao, H.; Guo, L.L.; Zeng, X.Y. Evaluation of bus vibration comfort based on passenger crowdsourcing mode. *Math. Probl. Eng.* 2016, *2016*, doi:10.1155/2016/2132454.
84. Sekulic, D. Influence of Road Roughness Wavelengths on Bus Passengers' Oscillatory Comfort. *Int. J. Acoust. Vib.* 2020, *25*, 41–53, doi:10.20855/ijav.2020.25.11512.
85. Liu, C.; Thompson, D.; Griffin, M.J.; Entezami, M. Effect of train speed and track geometry on the ride comfort in high-speed railways based on ISO 2631-1. *Proc. Inst. Mech. Eng. Part F J. Rail Rapid Transit* 2020, *234*, 765–778, doi:10.1177/0954409719868050.
86. Irvine, T. Vibrationdata Tutorial Page Available online: http://www.vibrationdata.com/tutorials.htm (accessed on May 4, 2021).
87. International Organization for Standardization ISO 8041 - Human response to vibration - Measuring instrumentation 2005.
88. Comité Européen de Normalisation EN 13803-1 - Railway applications - Track - Track alignment design parameters - Track gauges 1435 mm and wider - Part 1: Plain line 2010.
89. Liu, R.K.; Xu, P.; Sun, Z.Z.; Zou, C.; Sun, Q.X. Establishment of track quality index standard recommendations for beijing metro. *Discret. Dyn. Nat. Soc.* 2015, *2015*, doi:10.1155/2015/473830.
90. Kim, Y.G.; Choi, S.; Kim, S.W.; Kim, Y.M.; Park, T.W. An experimental study on the ride comfort of the Korean high-speed train. *Exp. Tech.* 2009, *33*, 30–37, doi:10.1111/j.1747-1567.2008.00419.x.
91. Offenbacher, S.; Neuhold, J.; Veit, P.; Landgraf, M. Analyzing major track quality indices and introducing a universally applicable TQI. *Appl. Sci.* 2020, *10*, 1–17, doi:10.3390/app10238490.
92. Comité Européen de Normalisation EN 13848-5 - 2008+A1 Railway applications - Track - Track geometry quality - Part 5: Geometric quality levels - Plain line. 2010.